

# **MULTI-WAVELENGTH, EFFICIENT MID-IR LASER SYSTEM**

**PHASE I STTR**

**FINAL REPORT**

**Contract Number DASG60-97-M-0206**

**Reporting Period: July 25, 1997 to June 15, 1998**

**Sponsored by: ARPA/BMDO Innovative Science and Technology Office**

**Managed by: U S Army Space and Strategic Defense Command**

**Principal Investigator: Dr. Hanna Hoffman**

**LASERGENICS CORPORATION  
6830 Via Del Oro, Suite 103  
San Jose, CA 95119**

**DISTRIBUTION STATEMENT A  
Approved for Public Release  
Distribution Unlimited**

The views and conclusions contained in this document are those of the authors and should not be interpreted as necessarily representing the official policies, either expressed or implied, of the Government.

**20000802 154**

## REPORT DOCUMENTATION PAGE

Form Approved  
OMB No. 0704-0188

1a. REPORT SECURITY CLASSIFICATION unclassified		1b. RESTRICTIVE MARKINGS	
2a. SECURITY CLASSIFICATION AUTHORITY		3. DISTRIBUTION/AVAILABILITY OF REPORT unlimited	
2b. DECLASSIFICATION/DOWNGRADING SCHEDULE			
4. PERFORMING ORGANIZATION REPORT NUMBER(S)  LGC-11		5. MONITORING ORGANIZATION REPORT NUMBER(S)	
6a. NAME OF PERFORMING ORGANIZATION Lasergenics Corp.	6b. OFFICE SYMBOL (If applicable)	7a. NAME OF MONITORING ORGANIZATION U. S. Army Space and Strategic Defense Command	
6c ADDRESS (City, State, and ZIP Code)  6830 Via Del Oro, Ste. 103 San Jose, CA 95119		7b. ADDRESS (City, State, and ZIP Code) P. O. Box 1500 ATTN: CSSD-TC-AE Huntsville, AL 35807-3801	
8a. NAME OF FUNDING/SPONSORING ORGANIZATION DARPA/BMDO Innovative Science and Technology Office	8b. OFFICE SYMBOL (If applicable)	9. PROCUREMENT INSTRUMENT IDENTIFICATION NUMBER DASG60-97-M-0206	
8c ADDRESS (City, State, and ZIP Code)  ATTN: Director, Directed Energy 7100 Defense Washington, DC 20310-7000		10. SOURCE OF FUNDING NUMBERS	
		PROGRAM ELEMENT NO.	PROJECT NO.
		TASK NO.	WORK UNIT ACCESSION NO.
11. TITLE (Include Security Classification)  Multi-wavelength, Efficient Mid-Infrared Laser System			
12. PERSONAL AUTHOR(S) Dr. Hanna Hoffman, Dr. Hans Jennisn			
13a. TYPE OF REPORT Final	13b. TIME COVERED FROM 7/97 TO 6/98	14. DATE OF REPORT (Year, Month, Day) 98-6-15	15. PAGE COUNT 72
16. SUPPLEMENTARY NOTATION			
17. COSATI CODES		18. SUBJECT TERMS (Continue on reverse if necessary and identify by block number)  Cascade Laser, Ho:YLF, Ho:BYF, Fibers, Single Crystal, Modelling, Spectroscopy, Cross-Relaxation, 4 μm	
19. ABSTRACT (Continue on reverse if necessary and identify by block number)  The objective of this project was to investigate the feasibility of producing radiation at multiple wavelengths from a single solid state laser medium. We investigated holmium doped YLF and BYF. Both the growth of boules and single crystal fiber growth were investigated. Laser quality boules of high Ho concentration were grown. Although single crystal fibers were grown, they were not of laser quality due to oxygen contamination. Improvements in the laser modeling of this system were made which included cross relaxation of several levels and resonant pumping of more than one level. Cascade laser action was investigated with the model which incorporated the measurement of several absorption cross sections, fluorescence lifetimes and cross relaxation rates that were measured during the course of the program. In laser tests, lasing was observed at 1.4 μm and 750 nm with very low thresholds observed at 1.4 μm.			
20. DISTRIBUTION/AVAILABILITY OF ABSTRACT <input checked="" type="checkbox"/> UNCLASSIFIED/UNLIMITED <input type="checkbox"/> SAME AS RPT. <input type="checkbox"/> DTIC USERS		21. ABSTRACT SECURITY CLASSIFICATION unclassified	
22. NAME OF RESPONSIBLE INDIVIDUAL Dr. Richard Schlecht		22b. TELEPHONE (Include Area Code) (408) 363-9791	22c. OFFICE SYMBOL

## TABLE OF CONTENTS

<u>Section</u>	<u>Title</u>	<u>Page</u>
1.	Introduction	1
2.	Mid-IR Laser Concept and Analysis	5
	2.1 Resonantly Pumped Cascade Laser Concept - a Review	5
	2.2 Cascade Laser Modelling	12
3.	Material Growth and Fabrication	20
	3.1 Ho:BYF Growth and Fabrication	20
	3.2 Fluoride Fiber Crystal growth	20
4.	Experimental Studies	32
	4.1 Spectroscopic Evaluations	32
	4.1.1 Absorption Spectra	32
	4.1.2 Fluorescence Emission and Excitation Spectra	35
	4.1.3 Lifetime Measurements	44
	4.2 Z-scan Fluorescence Experiments	47
	4.3 Short Pulse Laser Experiments	63
5.	Conclusions	67
	References	69

## I. Introduction

Numerous DOD programs require a frequency agile mid-IR laser operating at one or several different wavelengths spanning the 2-5  $\mu\text{m}$  range and beyond. Applications include illumination for space based lasers, imaging, countermeasures, remote sensing, eye-safe lidars, environmental agent detection and global wind sensing, to name a few. In some of these applications, the laser is required to operate in a cw or quasi-cw mode, while others dictate a pulsed mode with nanosecond pulse output. Other requirements may include overall good beam quality and multi-wavelength capability. In most cases, the laser source must be scalable to average powers in excess of 10 W and have the potential for high efficiency, all from a compact and ruggedized package. To meet such demanding sets of requirements it is generally accepted that a mid-IR source based on some solid state laser is the preferred technology path, especially for field applications where reliability is a crucial feature.

Existing solid state mid-infrared lasers are, however, of limited capability and usually fall short in one or more areas. For example, holmium and erbium doped lasers are available with output wavelengths at 2 and 3  $\mu\text{m}$ , respectively. Though both types of lasers are scalable to high average powers, they do not provide any spectral agility and/or wavelength tunability. In recent years, the main options considered for producing frequency-agile lasers in the mid-IR, especially beyond 3  $\mu\text{m}$ , were directed at down-shifting some shorter wavelength radiation using a nonlinear conversion process such as an optical parametric oscillator (OPO) or Raman conversion. While capable of providing wavelengths beyond 3  $\mu\text{m}$ , frequency conversion methods suffer from a number of drawbacks, including optical system complexity and degraded reliability due to potential damage to the nonlinear crystal used for an OPO or beam quality degradation in the case of Raman shifting in gases. Furthermore, both methods generally require a high peak power (i.e., short pulse) pump laser for efficient radiation conversion. Consequently they do not lend themselves well to cw or quasi-cw applications, especially for applications where higher average powers are required as well.

The purpose of this Phase I STTR project was to establish feasibility of a promising alternative approach to producing radiation at multiple wavelengths in the mid-IR, including at wavelengths beyond 3  $\mu\text{m}$ , all from a single solid state laser medium. The laser concept is based on a novel combination of resonant pumping and cascade laser transitions, inspired by experiments conducted in the late seventies by Esterowitz et al<sup>1</sup> and by

Eckart et al<sup>2</sup> and more recently extended by Dr. Hans Jenssen who suggested the possibility of exploiting certain cross relaxation processes thereby allowing quasi-cw pumping. Thus, while laser transitions in Ho:YLF were successfully demonstrated at several mid-IR wavelengths, including at 2.9  $\mu\text{m}$  and 3.9  $\mu\text{m}$ , using pulsed pumping in the green<sup>1,2</sup>, the self-terminating nature of these transitions limited their practical utility to lower repetition rates (below 10 Hz). A strong laser transition at 750 nm was also demonstrated in Ho:YLF using 532 nm laser pumping<sup>3</sup>. Prior to the start of this project, analysis of holmium-doped fluorides by Dr. Jenssen indicated that under certain circumstances, the Ho<sup>3+</sup> ion level transition dynamics is such that a fortuitous three-photon absorption process at 750 nm could take place in certain hosts, providing a mechanism for achieving effective inversion upon pumping with quasi-cw radiation. This raised the possibility of achieving the same laser transitions seen in Refs. 1 and 2, but with scalable power outputs, and using a pumping wavelength accessible with efficient diode arrays.

On a previous SBIR project (Navy Contract No. N00024-96-C-4166), on which Dr. Jenssen served as a key consultant, Ho:YLF was investigated as a candidate material in the hope of demonstrating a three-photon absorption process at 750 nm, that could lead to a practical 4  $\mu\text{m}$  laser device. At the conclusion of that project, it was determined that at higher Ho ion concentrations (over 10%), a strong cross relaxation process does indeed take place, allowing for efficient two-photon absorption at 750 nm. Unfortunately, the critical third excited state absorption (from the lower level of the 4  $\mu\text{m}$  transition) was found to have too low a cross section for efficient lasing at 4  $\mu\text{m}$  with only a 750 nm pump at realistic power levels. A number of alternative mechanisms were suggested, including the use of a second pump wavelength near 1.02  $\mu\text{m}$  or lasing the 3  $\mu\text{m}$  line in a cascade with the 4  $\mu\text{m}$  transition. It was also recognized that an alternative fluoride system, namely Ho:BaY<sub>2</sub>F<sub>8</sub> (Ho:BYF) would be a better candidate material than Ho:YLF for exploring the mid-IR transitions of interest due to more favorable spectroscopic properties.

Thus, preliminary analysis of Ho:BYF by Dr. Jenssen prior to the start of this program predicted that it may possess longer upper laser level lifetimes and higher relative gains than those of Ho:YLF. This material was used in the past to demonstrate lasing on the  $^5\text{F}_5 \Rightarrow ^5\text{I}_5$  transitions near 2.4  $\mu\text{m}$  using flashlamp pumping at low temperatures and there were indications that the  $^5\text{I}_6 \Rightarrow ^5\text{I}_7$  transition at 2.9  $\mu\text{m}$  can also be readily lased if the self-termination problem could be overcome<sup>4</sup>. There had been, however, relatively little work performed with Ho:BYF and its level structure and key material

parameters were not as well known as with the more familiar Ho:YLF. Also the growth process for Ho:BYF is somewhat more difficult compared to Ho:YLF and its monoclinic structure makes selection of the most favorable orientations somewhat more difficult.

The need to resolve these issues coupled with the promise of Ho:BYF as a material of choice for exploring mid-IR laser transitions led to this STTR project which was conducted as a close collaboration between Lasergenics Corporation and CREOL at the University of Central Florida (UCF). Most of the material growth and characterization efforts were carried out at CREOL by Dr. Jenssen, assisted by several of his students, who contributed some of the key results achieved on this project.

The primary goal set for the Phase I project was to explore feasibility of producing radiation at several key wavelengths in the mid-IR, most notably at 4  $\mu\text{m}$ , from Ho:BYF crystals grown specifically for this effort. The project was expected to benefit from the availability of measurement data, equipment and previously grown samples of Ho:YLF acquired on a previous Phase I SBIR project and useful for comparative purposes.

Specific objectives set for this Phase I project were three-fold: 1). to determine Ho:BYF material parameters most optimal for producing direct laser emission at 4  $\mu\text{m}$  and other IR wavelengths including 3  $\mu\text{m}$  and 1.4  $\mu\text{m}$ , using resonant pumping at or near or 750 nm. These pump photons could be provided, for example, by a Ti:sapphire or an alexandrite pump laser in the near-term and, ultimately by diode arrays in the longer term; 2.) to demonstrate lasing at 0.75  $\mu\text{m}$ , 1.4  $\mu\text{m}$  and possibly at 3.9  $\mu\text{m}$  from Ho:BYF using a short pulse green laser pump, similar to the early demonstrations conducted for Ho:YLF<sup>1,2,3</sup> and; 3.) to investigate prospects for growing holmium-doped crystal fibers using the Laser-Heated Pedestal-Growth technique (LHPG). The motivation for this objective was that the fiber geometry is known to be a highly effective means for achieving lower thresholds even in lower gain three-level systems. It is also well matched to diode end-pumping, which is the configuration ultimately favored for a resonantly pumped cascade laser. Furthermore, even though each fiber may be limited in output power, the combination of individual beam outputs in parallel is a potentially promising technique for scaling the overall laser output power from this structure.

The basic approach designed to meet the project objectives consisted of material growth (fiber and bulk) and sample fabrication, level modelling and analysis, spectroscopic measurements and proof-of-concept laser experiments. Following this approach, during the course of Phase I, we have:

- successfully grown two high quality boules of Ho:BYF with different concentrations,
- modified the model to include revised material parameters and improve its predictive capability,
- performed a series of spectroscopic measurements verifying the existence of strong cross relaxation processes in Ho:BYF,
- demonstrated lasing at 0.75 and 1.4  $\mu\text{m}$  using a 10 ns pump laser at 532 nm, and
- investigated issues pertaining to growth of fluoride crystal fibers using the LHPG method.

Preliminary conclusions point to the feasibility of producing 3  $\mu\text{m}$  radiation from Ho:BYF at practical 750 nm input pump power levels. Such a laser could be useful as an alternative to Er-doped lasers in applications where diode pumping is important. Prospects for producing the desired 4  $\mu\text{m}$  radiation appear best if the transition is lased in sequence with the 3  $\mu\text{m}$  line. This possibility is therefore recommended for further investigation. As a side benefit we have also demonstrated, somewhat unexpectedly, that gain switched radiation at 1.4  $\mu\text{m}$  could be produced with very low threshold and high slope efficiency using a short pulse green laser pump. Since the repetition rate for such a laser is scalable to possibly even beyond 50 Hz, this could be a potentially useful laser in applications requiring eye safe radiation as well as in medical surgery and diagnostics, communications and spectroscopy. The frequency doubled wavelength near 0.7  $\mu\text{m}$  could, in addition, find uses in surgical applications requiring a red wavelength such as photodynamic therapy and tattoo removal among others.

Summary of the work accomplished on the project tasks is reported in what follows.

## II. Mid-IR Laser Concept and Analysis

### 2.1 Resonantly Pumped Cascade Laser Concept - a Review

It is well known that the Ho ions are capable of producing stimulated emission at several wavelengths across the infrared. Figure 2.1 shows the characteristic energy level diagram indicating the large number of transitions that exhibited fluorescence and/or laser emissions under a variety of pumping conditions. Since the energy levels in fluorides are spaced sufficiently apart, the non-radiative relaxation processes are not too strong. The consequent fluorescence can be made to lase, provided lifetimes and emission cross sections are of the proper magnitude. However, apart from the customary transition at 2.1  $\mu\text{m}$  from the  $^5\text{I}_1$  level to the ground state, other higher level transitions can be very difficult to lase using standard excitation techniques such as flashlamps which, being broad-band, require upper laser levels with long fluorescent lifetimes and small nonradiative decay rate. Yet, some of the most interesting laser transitions such as the 4  $\mu\text{m}$  one between  $^5\text{I}_6$  and  $^5\text{I}_5$  originate on levels characterized by lifetimes that are short compared with those of the lower levels. This effectively turns the transition into a three-level laser system, resulting in very high thresholds and self terminating laser action. Other difficulties associated with long wavelength transitions include rapid multiphonon nonradiative decay rates between closely spaced levels and smaller stimulated emission cross sections.

One way to force laser action under such unfavorable conditions is to cool the gain material, since at lower temperatures the non-radiative transition rates decrease, thereby increasing upper level lifetimes and reducing reabsorption losses, resulting in lower lasing thresholds. Another option, which avoids the need for cooling, is through use of short pulse resonant pumping. With direct excitation to the upper laser level, a population inversion can be created even from levels where long fluorescence lifetimes are not available, thus circumventing the limitation suffered by broadband excitation techniques. Furthermore, in certain cases, advantage can be taken of cascade processes whereby laser oscillation between intermediate levels is exploited to increase the rate of transition to the upper level of a lower-lying manifold thus achieving inversion on an otherwise unfavorable laser transition, and resulting in multi-wavelength sequential emission. A cascade action, where one laser transition effectively pumps a lower laser transition in the same material, can also help reduce losses associated with alternative modes of decay - both

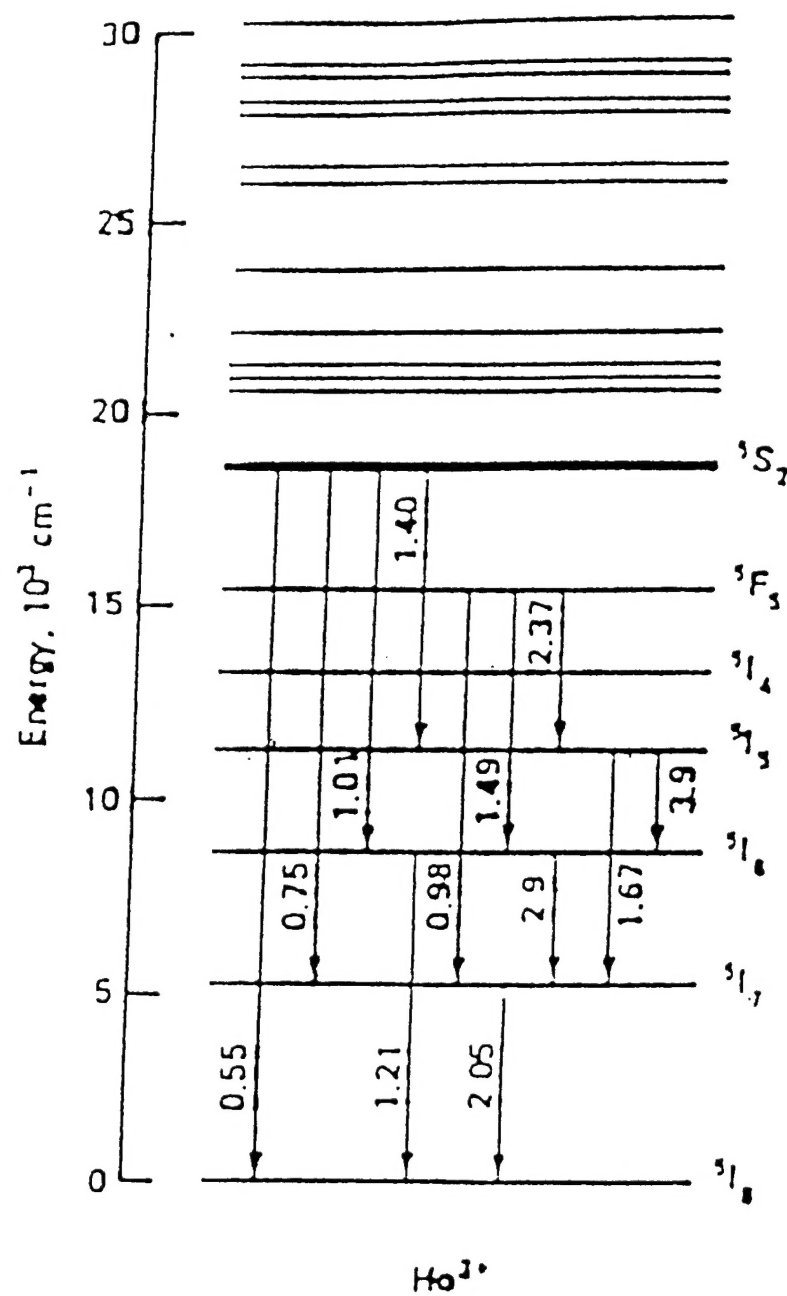


Figure 2.1 Level Diagram of  $\text{Ho:YLF}$  Showing Wavelengths (in  $\mu\text{m}$ ) of Observed Laser Transitions

radiative and non-radiative (e.g., multi-phonon relaxation) - thereby further improving the efficiency of intermediate laser transitions.

While advantageous from a laser dynamics viewpoint, resonant pumping does require a laser tuned to an appropriate absorption line of the laser material. In the case Ho:YLF, cascade laser action at several lines in the mid-IR was obtained by resonantly pumping the  $^5I_8$  ground state to the  $^5S_2$ ,  $^5F_4$  levels using a green beam tuned to the absorption for these levels<sup>1-3</sup>. In particular, using a short pulse green 535.5 nm radiation from the second harmonic of a Nd:glass laser to transversely pump a 1% Ho:YLF crystal, laser action was successfully demonstrated by Esterowitz et al<sup>1</sup> on both the 1.4  $\mu\text{m} \Rightarrow 3.9 \mu\text{m}$  and the  $1.4 \Rightarrow 1.7 \mu\text{m}$  cascade transitions, all at room temperature. In these early experiments a relatively high pump intensity was required to activate the 3.9  $\mu\text{m}$  transition, in keeping with its long lived lower laser level lifetime. Shortly thereafter, Eckart et al<sup>2</sup> reported a three-line sequential laser emission at 3.4  $\mu\text{m}$ , 3.9  $\mu\text{m}$  and 2.9  $\mu\text{m}$ , also in Ho:YLF, but using the 535.5 nm laser emission from a pulsed dye laser with a 1  $\mu\text{s}$  long pulse.

However, these transitions, while interesting, have limited utility in most practical settings, because repetition rates are fundamentally limited when there are low lying states with long fluorescence lifetimes, even with short pulse pumping and cascade lasing. Generally, as the repetition frequency is increased close to the inverse of the lower level lifetime, a bottleneck is created, and laser action becomes self-terminating. Such is indeed the case for Ho:YLF where pumping with a green beam to the  $^5S_2$  manifold is followed by a laser transition to the long lived ( $> 2 \text{ msec}$ )  $^5I_5$  level (whether through the 1.4  $\mu\text{m}$  transition as in Ref. 1 or through 2.37  $\mu\text{m}$  as in Ref. 2). This, coupled with the fact that the  $^5I_6$  eventually decays to the  $^5I_7$  which is even longer lived at  $>10 \text{ msec}$  lifetime, creates a bottleneck, terminating laser action as repetition rates are increased. This limits operation under short pulse pumping to lower repetition rates ( $< 10-20 \text{ Hz}$ ) and also results in high thresholds for both the 3.9 and 2.9  $\mu\text{m}$  transitions.

To extend mid-infrared laser operation from intermediate holmium levels to higher repetition rates, or even to the cw regime, a mechanism must be found to empty the population in the long lived lower energy levels, thereby maintaining population inversion by effectively reducing level lifetimes. Such a mechanism does, in fact, take place in certain rare earth doped host materials due to favorable coincidences between cross relaxation and/or excited state absorption processes. For example, in high

concentration erbium-doped lasers, the 3  $\mu\text{m}$  transition is feasible precisely because of such ion-ion cross-relaxation processes.

Motivating this project was the hope that similarly favorable conditions may exist for lasing the 4  $\mu\text{m}$  transition between the  $^5\text{I}_5$  and  $^5\text{I}_6$  levels in  $\text{Ho}^{3+}$  doped BYF. Preliminary indications based on prior calculations by Dr. Jenssen indicated that a fortuitous coincidence between ground state and excited states absorptions on the one hand, coupled with favorable cross-relaxation processes, may indeed favor a sequential lasing transition to the  $^5\text{I}_6$  level upon pumping with a single wavelength at or around 750 nm. In a previous work, Knight et al<sup>3</sup> used a 532 nm beam from a frequency doubled, Q-switched Nd:YAG laser to pump Ho:YLF, resulting in short pulse radiation at 750 nm at repetition rates as high as 40 Hz, all at room temperature and with excellent efficiency. From these experiments it was inferred that the 750 nm transition from the  $^5\text{I}_7$  level to  $^5\text{S}_2$  in Ho:YLF is a strong one, with an emission cross section on the order of  $10^{-19} \text{ cm}^2$ . The absorption cross section for the same transition is therefore expected to be of similar magnitude. The ground state absorption  $^5\text{I}_8 \Rightarrow ^5\text{I}_4$  is known to exist at the same wavelength but is much weaker, with a cross section of only about  $10^{-22} \text{ cm}^2$ .

Prior spectroscopic studies by Dr. Jenssen also pointed to the intriguing possibility that a third absorption process from the  $^5\text{I}_6$  may exist at the same wavelength, which would make it possible to break the bottleneck on the  $^5\text{I}_5 \Rightarrow ^5\text{I}_6$  transition at 4  $\mu\text{m}$ , using a single wavelength pump. Such a three-photon absorption would also be instrumental in lowering thresholds for laser operation, avoiding self-termination at higher repetition rates and allowing operation in a quasi-cw mode. A previous SBIR Phase I project was awarded by the Navy to investigate this concept, especially as it applies to potential scaled-up laser operation near 4  $\mu\text{m}$ .

The key elements of that concept are shown in Figure 2.2. As indicated, radiation at 750 nm is used to pump the  $\text{Ho}^{3+}$  ion in YLF or BYF to a high lying level through a three photon absorption process, followed by emission at 3.9  $\mu\text{m}$  in a cascade with the 1.4  $\mu\text{m}$  laser transition from  $^5\text{S}_2$ . Alternatively, cross relaxation processes involving higher lying levels of the active ion, as shown in Figure 2.3, may also favor the 3.9  $\mu\text{m}$  transition, with or without a cascade. In either case there is potential for highly efficient 3.9  $\mu\text{m}$  laser action. In the first scenario, the simplest option is to allow the population in the  $^5\text{S}_2$  level to accumulate until it reaches a level high enough for the 1.4  $\mu\text{m}$  laser transition to be Q-switched, thereby gain switching the 4  $\mu\text{m}$  cascade transition from the  $^5\text{I}_5$  level. One positive indication supporting a

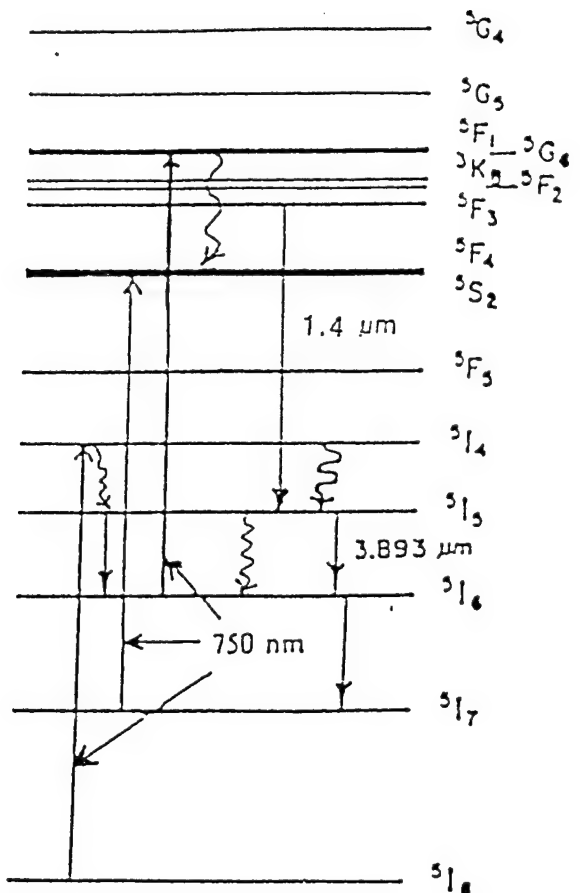


Figure 2.2 Potential 3-photon 750 nm Absorption and 1.4  $\Rightarrow$  3.9  $\mu\text{m}$  Cascade Lasing in Ho:YLF

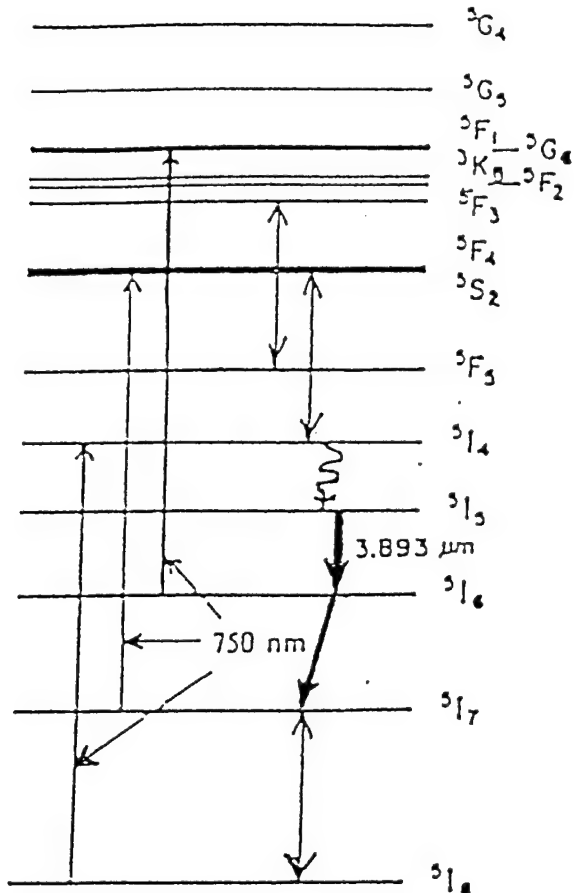


Figure 2.3 Potential for lasing at 3.9  $\mu\text{m}$  following 3-photon 750 nm Absorption and 2 Cross Relaxation Processes

practical application of this approach is the relatively high gain of the 1.4  $\mu\text{m}$  transition, which was successfully produced at room temperature using flashlamp pumping<sup>5</sup>. In the second scenario, favorable cross relaxation processes are sought, which are expected to become more prominent as the concentration of the active ion increases. The two predicted cross relaxation processes involve the transitions  $^5F_3 \Rightarrow ^5F_5$ ,  $^5I_8 \Rightarrow ^5I_7$ , and  $^5S_2 \Rightarrow ^5I_4$ ,  $^5I_8 \Rightarrow ^5I_7$  which help populate the upper  $^5I_5$  laser level, thus contributing to population inversion through recycling of the pump photons.

The two key questions for the earlier SBIR project were therefore the viability of a three photon absorption process in Ho:YLF and the relative strength of cross relaxation processes as a function of the holmium ion concentration. Substantial modeling and spectroscopic evaluations were carried out at CREOL's facilities using Ho:YLF as the primary material. In particular, it was hoped that the 750 nm absorption cross section from  $^5I_6$  to the  $^5F_3$  manifold (which was not apriori known) would be of the same magnitude as the  $^5I_7 \Rightarrow ^5S_2$  absorption, i.e., about  $10^{-19} \text{ cm}^2$ . This, however, turned out not to be the case. Specifically, the absorption cross section for the  $^5I_6 \Rightarrow ^5S_2$  transition was found to be less than  $5 \times 10^{-22} \text{ cm}^2$  which meant that pumping at 750 nm alone will not be sufficient to achieve and maintain population inversion on the 4 micron line except at very high pump power densities (on the order of  $100 \text{ kW/cm}^2$ ). This is because, with such a weak absorption, the lower laser level would not be de-excited fast enough to overcome the population build-up due to the short upper state lifetime, resulting effectively in a three level process.

On the other hand, both modeling and spectroscopic measurements provided evidence of a strong 2-photon absorption at 750 nm, validating previous expectations. There was however encouraging evidence that the desired cross relaxation processes do indeed take place with an efficiency that increases with increasing  $\text{Ho}^{3+}$  concentration, thereby providing a potential mechanism for rapidly populating the  $^5I_5$  upper laser level. This led to the conclusion that with holmium doping levels on the order of 10%, it may not be necessary to lase the  $^5S_2 \Rightarrow ^5I_5$  transition at 1.4  $\mu\text{m}$  as a means to trigger a cascade transition at 4  $\mu\text{m}$ . This could lead to a simpler overall laser design, and further investigation of this possibility was therefore strongly recommended.

Unfortunately, further temporal evolution and spectroscopic measurements indicated that, even with favorable cross relaxation increasing the upper  $^5I_5$  level population, additional mechanisms must be

found to also reduce the population of the long lived  $^5I_6$  lower laser state for inversion to be achieved at reasonable pump power density levels. In that previous project the two most promising means identified to achieve this were 1.) to lase the 3  $\mu\text{m}$  transition to the lower lying  $^5I_7$  level in a cascade with the 4  $\mu\text{m}$  laser, and/or 2.) to utilize a second pump wavelength to excite electrons in  $^5I_6$  up to some higher lying level. For example, the 1.01  $\mu\text{m}$  transition from  $^5I_6$  to  $^5S_2$  could be used, from which level energy would be efficiently transferred to the  $^5I_5$  upper laser level through radiative decay aided by cross relaxation. Further modeling as well as spectroscopic studies were therefore recommended to explore both of the above options.

Another option suggested was to explore an alternative fluoride system such as Ho:BYF, where longer upper level lifetimes are expected. For example, with lower multiphonon relaxation rates, Ho level lifetimes in this host were measured by Dr. Jenssen to be about 70  $\mu\text{s}$  for  $^5I_5$  and 300  $\mu\text{s}$  for  $^5S_2$  - considerably larger than in YLF. This could improve prospects for achieving population inversion, even in the absence of a strong absorption from the  $^5I_6$  level. However, there has been relatively little experimental work performed using Ho:BYF, and parameters for this material, including most relevant absorption cross sections and excited state transitions, were not well known. Neither were the relative strengths and contribution of cross relaxation processes measured prior to the present work. Such measurements therefore became a key objective in the present work, which concentrated on modeling and experimental characterization of Ho:BYF samples grown specifically for this Phase I project (this material is not currently commercially available).

At the onset of this project the following key issues were identified as critical to the successful demonstration of our objectives. In particular, we set out to:

1. Measure the absorption of Ho:BYF as a function of concentration at around 750 nm and also at 532 nm. Estimate the absorption cross sections and use as input to the model.
2. Determine whether strong cross relaxation exist in Ho:BYF similar to Ho:YLF and what the dependence on concentration is. In particular, it was expected that cross-relaxation quenching of the  $^5S_2$  level makes the lifetime of this level concentration dependent, and this is a critical input into the model.
3. Determine whether cascade lasing can be effectively used as a

means of rapidly populating the upper 4  $\mu\text{m}$  laser level, especially in the presence of cross relaxation processes.

4. Provide preliminary indications as to the possible existence or absence of competing excited state absorption (ESA) processes, especially from the  $^5\text{I}_5$  and/or  $^5\text{S}_2$ .
5. Identify alternatives whereby the lower laser level of the  $^5\text{I}_5 \Rightarrow ^5\text{I}_6$  transition of interest can be depopulated, for example by exploiting the 2.9  $\mu\text{m}$  transition to the lower (and longer lived)  $^5\text{I}_7$  level in a cascade with the 4  $\mu\text{m}$  transition.

The effort reported herein was limited to preliminary study of some key issues of Ho:BYF through modeling, analysis, related spectroscopic measurements and some initial laser testing as allowed by materials and equipment at hand. The latter testing was to include both direct pumping with pulsed green photons and possibly cw pumping with an available 750 nm laser, provided sufficient power is available. These are discussed in Section V below. The remainder of this section is concerned with results of modeling performed on the project.

## 2.2 Cascade Laser Modelling

Given the complexity and variety of the closely spaced levels of the Ho ion, the energy transfer model required to fully parametrize all the processes is quite complicated. On the previous SBIR project, a model was developed to characterize the dynamics of energy transfer throughout the Ho excitation levels for the case of resonant pumping of Ho:YLF at 750 nm. Three photon excitation was included using a combination of known and newly derived spectroscopic parameters. The model was later extended to partially include contributions from cross relaxation terms and more recent data. Computations were also reformatted to run on both Mathematica and Microsoft Excel programs. At the onset of this project, the model, in its current format, allowed determination of pumping rates and intensities required to saturate the critical  $^5\text{I}_6 \Rightarrow ^5\text{G}_6$  transition as well as the rates of population build-up at various levels of interest as a function of input pump power. Using input data on level lifetimes and branching ratios, the threshold fluxes for achieving inversion on the 4  $\mu\text{m}$  transition could be calculated for given Ho concentrations and compared with experiment, with good agreement.

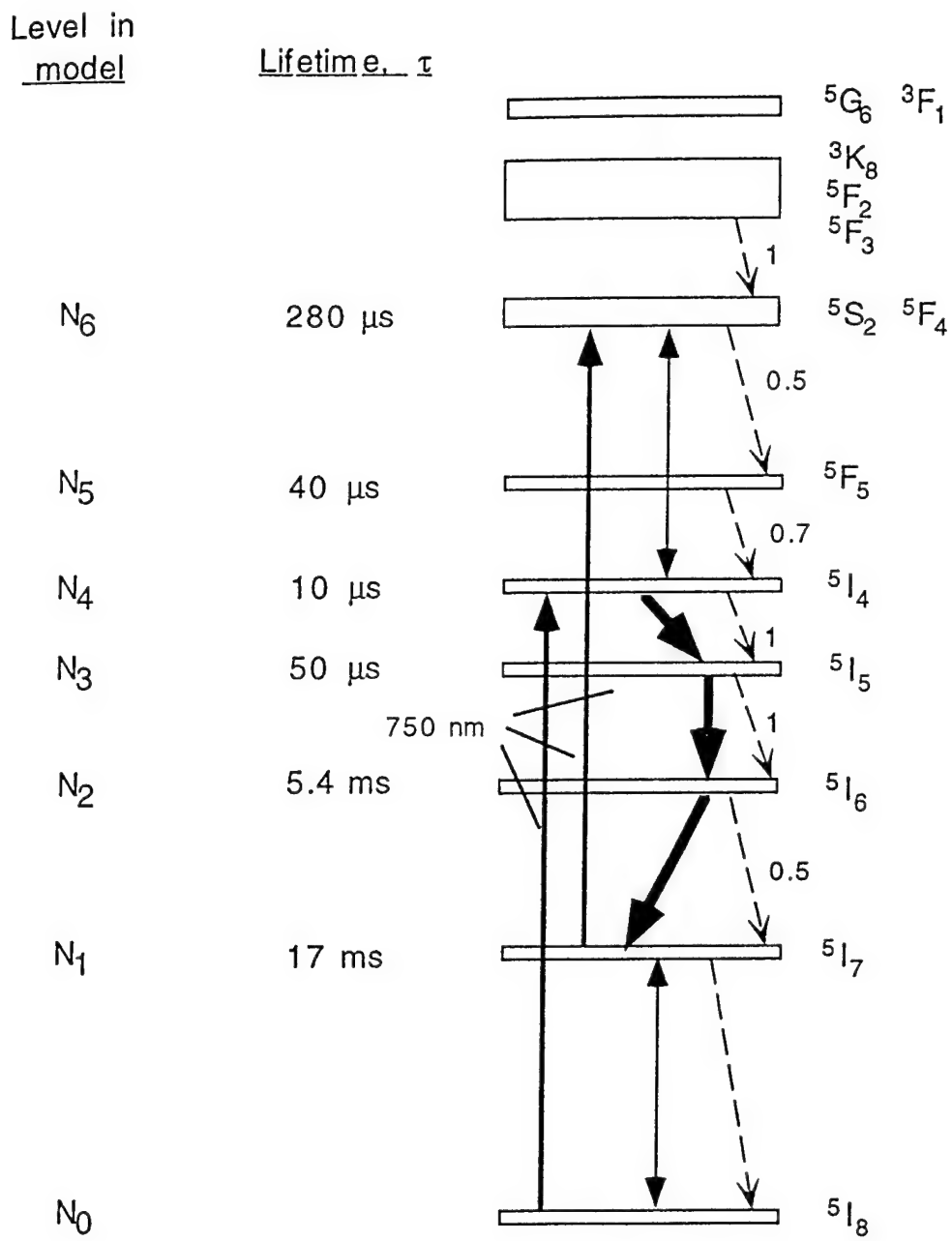
On this Phase I project the model was further upgraded to more fully include the effects of cross relaxation and to also accomodate the possibility of direct resonant pumping of more than one level. In addition, a method was devised for estimating the effect of lasing at 3  $\mu\text{m}$  from the lower lying level of the 4  $\mu\text{m}$  transition. To counter these added complications, the previous system of 8 coupled equations was limited to the contributions of only the first 7 levels of Ho:BYF. Also, in keeping with earlier results indicating low absorption cross sections for the  $^5\text{I}_6$  level, only a two-photon absorption at 750 nm was included.

Figure 2.4 shows the relevant energy levels of the Ho ion in BYF along with the absorption and cross relaxation processes relevant to this system. Some of the key fluorescence level lifetimes, decay rates, and branching ratios indicated for the various levels were measured as part of this project while others were estimated from comparison with Ho:YLF.

To describe the energy transfer dynamics in a Ho:BYF system the following set of seven coupled differential rate equations is used:

$$\begin{aligned}
 N_0 &= C_{\text{Ho}} - N_1 - N_2 - N_3 - N_4 - N_5 - N_6 \\
 dN_1/dt &= -\sigma_{16}R_{16}N_1 - N_1/\tau_1 + 0.5 N_2/\tau_{2,1} + N_6 / \tau_{\text{CR}} + \\
 &\quad \sigma_{12}R_{12}(N_2 - g_2N_1/g_1) \\
 dN_2/dt &= -\sigma_{26}R_{26}N_2 - N_2/\tau_2 + N_3/\tau_{3,2} - \sigma_{12}R_{12}(N_2 - g_2N_1/g_1) \quad (1) \\
 dN_3/dt &= -N_3/\tau_3 + N_4/\tau_{4,3} \\
 dN_4/dt &= \sigma_{04}R_{04}N_0 - N_4/\tau_4 + 0.7 N_5/\tau_5 + N_6 / \tau_{\text{CR}} \\
 dN_5/dt &= -0.7N_5/\tau_5 + 0.5 N_6/\tau_{6,5} \\
 dN_6/dt &= \sigma_{16}R_{16}N_1 + \sigma_{26}R_{26}N_2 - 0.5 N_6/\tau_6 - N_6 / \tau_{\text{CR}}
 \end{aligned}$$

where  $C_{\text{Ho}}$  is the concentration of holmium ion in  $\text{cm}^{-3}$ ,  $\sigma_{ij}$  are absorption or emission cross sections as shown in Figure 2.4,  $R_{ij}$  are pumping rates from level  $i$  to level  $j$ ,  $\tau_i$  are level  $i$  lifetimes also shown in the figure and  $\tau_{ij}$  are the inverse relaxation rates from level  $i$  to  $j$ . These equations also include nonlinear terms due to the cross relaxation processes:  $^5\text{F}_4 \Rightarrow ^5\text{I}_4 + ^5\text{I}_7$  and  $^5\text{F}_3 \Rightarrow ^5\text{F}_5 + ^5\text{I}_7$ . Cross-relaxation processes become a significant effect at higher Ho ion concentrations, which for the sample calculations performed



$$\sigma_{16} = \sigma(^5I_7 \rightarrow ^5S_2) = 4 \times 10^{-20} \text{ cm}^2$$

$$\sigma_{04} = \sigma(^5I_8 \rightarrow ^5I_4) = 8 \times 10^{-23} \text{ cm}^2$$

FIGURE 2.4: Energy levels and transfer parameters for the 3.9  $\mu m$  Ho:BYF laser as used in model calculations

are 10% and 20%. In this case, the cross-relaxation lifetime  $\tau_{CR}$ , which is proportional to the ground state population  $N_0$ , is assumed to be about 5  $\mu\text{s}$  (the same for both processes for simplicity).

Cross relaxation rates increase with concentration. This shortens the lifetime of the  $^5S_2$  level by rapid relaxation from  $^5S_2$  to  $^5I_4$ , followed by multiphonon relaxation from  $^5I_4$  to  $^5I_5$ , and efficiently contributes to the build up in the population of the upper laser level ( $^5I_5$ ) of the 4  $\mu\text{m}$  laser transition. The cross relaxation rate can be determined by observing the change in the lifetime of the  $^5S_2$  manifold with changing Ho concentration. Using the lifetime measurement apparatus which will be described later, we directly pumped the  $^5S_2$  manifold with a pulsed Nd:YAG laser and monitored the fluorescence to the ground state. The unquenched lifetimes of the  $^5S_2$  manifold were found to be  $\approx 100 \mu\text{sec}$  for Ho:YLF and  $\approx 280 \mu\text{sec}$  for Ho:BYF in low concentration (1%) samples. As the concentration of Ho was increased, the lifetime of the  $^5S_2$  manifold decreased dramatically:

- in 10% Ho:YLF it was  $\approx 8 \mu\text{sec}$ , in 20% Ho:YLF it was  $\approx 2.4 \mu\text{sec}$ ;
- in 10% Ho:BYF it was  $\approx 15 \mu\text{sec}$ , in 20% Ho:BYF it was  $\approx 3 \mu\text{sec}$ .

As also indicated in Figure 4, the values assigned to the absorption cross sections  $\sigma_{04}$  and  $\sigma_{16}$  are  $8 \times 10^{-23}$  and  $4 \times 10^{-20} \text{ cm}^2$ , respectively. These are consistent with experimental data on this project (see Section IV).

With the above parameter assignments, and using the set of coupled equations (1), the equations were solved for the case of threshold for 4  $\mu\text{m}$  lasing. Taking into account the concentration of  $\text{Ho}^{3+}$  ions, the initial population of the ground level was calculated. The original system of 7 coupled differential equations that describes the temporal behavior of the populations of the 7 energy levels is quite complex and solutions of that system are not always easy to interpret. That is why we have first simplified the model by reducing it to a fewer number of participating energy levels and then adding additional levels one by one.

In the first simplified model the pump term  $^5I_8 \Rightarrow ^5I_4$  was not taken into account. Instead, the assumption was made that there is an initial population in the  $^5I_7$  level, which is being pumped to the  $^5S_2$  level. Cross relaxation results in the  $^5I_8 \Rightarrow ^5I_7$  transition and simultaneously the  $^5S_2 \Rightarrow ^5I_4$  transition. The next assumption that was made was that the  $^5I_4$  level excitation relaxes to the  $^5I_7$  level. As a result, the single excitation of an ion from  $^5I_7$  to  $^5S_2$  results in two excitations in the  $^5I_7$  level (one due to

relaxation from the upper levels  $^5S_2 \Rightarrow ^5I_4 \Rightarrow ^5I_7$ , and the other due to cross relaxation ( $^5I_8 \Rightarrow ^5I_7$ ). The outcome depends on the quantum efficiencies of the processes. For example, with 90% quantum efficiency of cross relaxation ( $^5S_2 \Rightarrow ^5I_4$  and  $^5I_8 \Rightarrow ^5I_7$ ) and 90% quantum efficiency of multiphonon relaxation,  $^5I_4 \Rightarrow ^5I_7$ , one excitation from  $^5I_7$  to  $^5S_2$  results in 1.7 excitations in the  $^5I_7$  level.

By solving this simplified model we have come to the conclusion that the steady state population of the  $^5I_7$  level does not depend on the initial population in that level. At each given pump power at 750 nm the steady state value of the  $^5I_7$  population was the same whether we started with 10 ions in the  $^5I_7$  level or  $10^{21}$  ions. The higher the initial population of the  $^5I_7$  level, the faster the system came to steady state.

In this way we could also check on the significance of the pump term  $^5I_8 \Rightarrow ^5I_4$  (that we have neglected) for building up the steady state population in  $^5I_7$ . The final steady state values are not affected by pumping from the ground state. The transition  $^5I_8 \Rightarrow ^5I_4$  only provides population in the  $^5I_7$  level at the beginning of the process. Later, the other processes in the system (cross relaxation, pumping from  $^5I_7$  to  $^5S_2$ ) take over and bring the system to the same steady state populations.

The next step in the theoretical modeling of the system was the addition of the  $^5I_6$  level. Again we have assumed that there is only pumping at 750 nm from the  $^5I_7$  level to the  $^5S_2$  level and no pumping from  $^5I_8$  to  $^5I_6$ , some initial population in  $^5I_7$ , cross relaxation  $^5S_2 \Rightarrow ^5I_4$  and simultaneously  $^5I_8 \Rightarrow ^5I_7$  with a quantum efficiency of 90%. From the  $^5I_4$  level we have considered relaxation to  $^5I_6$  with a 90% quantum efficiency. The quantum efficiency of relaxation from the  $^5I_6$  level to the  $^5I_7$  level was assumed to be 50%.

The calculations for this system showed that with increasing pump power at 750 nm (from 3 mW up to 2 W power focussed to a 30  $\mu\text{m}$  spot diameter) the steady state values of the population in the  $^5I_6$  level continuously increases. Meanwhile, the steady state population in the  $^5I_7$  level first increases with power and then at 20 mW of input power it becomes equal to the  $^5I_6$  population. It then drops with increasing pump power. Therefore, starting from 20 mW there is a population inversion between  $^5I_6$  and  $^5I_7$ .

The  $^5I_6$  population builds up to quite high values due to the lifetime of the level (2 msec for Ho:YLF and 5 msec for Ho:BYF). The population in the  $^5I_7$ ,

level, however, decreases in spite of an even longer lifetime and feeding due to cross relaxation, since the increasing pump power efficiently empties the  $^5I_7$  level. The population inversion between the  $^5I_6$  and  $^5I_7$  levels starting from pump powers as low as 20 mW can be used for the depletion of  $^5I_6$  by lasing from  $^5I_6$  to  $^5I_7$ .

In the next model we have included the  $^5I_5$  level. Condition and assumptions were the following: some initial population in  $^5I_7$ , no pump from  $^5I_8$  to  $^5I_4$ , pumping at 750 nm from  $^5I_7$  to  $^5S_2$ , cross relaxation  $^5S_2 \Rightarrow ^5I_4$  and simultaneously  $^5I_8 \Rightarrow ^5I_7$ , both with 90% quantum efficiency. From the  $^5I_4$  level we have considered relaxation to  $^5I_5$  with 100% quantum efficiency and from  $^5I_5$  to  $^5I_6$  with the same 100% quantum efficiency. The quantum efficiency of relaxation from the  $^5I_6$  level to the  $^5I_7$  level was assumed to be 50%.

The results of this calculation showed that:

- 1) the steady state population of  $^5I_6$  continuously increases with increasing pump power and reaches  $\approx 1.11 \times 10^{21} \text{ cm}^{-3}$  at 2 W of pump power;
- 2) the steady state population of  $^5I_7$  becomes equal to the population of  $^5I_6$  at 21 mW of pump power and then decreases with increasing pump power and reaches  $\approx 1.14 \times 10^{18} \text{ cm}^{-3}$  at 2 W of pump power;
- 3) the steady state population of  $^5I_5$  is lower than the  $^5I_6$  population throughout the entire range of pump power (3 mW to 2 W) and it is also lower than the  $^5I_7$  population above 1 W pump power and it reaches  $\approx 4.9 \times 10^{18} \text{ cm}^{-3}$  at 2 W of pump power.

As we can see, CW pumping at 750 nm *alone* does not allow one to achieve inversion of the population between the  $^5I_5$  and  $^5I_6$  levels (upper and lower levels of the 4  $\mu\text{m}$  transition), therefore making lasing between these levels not possible under these circumstances.

The main problem to achieving laser operation at 4  $\mu\text{m}$  with CW pumping at 750 nm is the long lifetime of its lower level,  $^5I_6$ , compared to the lifetime of its upper  $^5I_5$  level which results in the so called bottleneck effect. The only way to break the bottleneck due to unfavorable lifetime ratios between  $^5I_5$  and  $^5I_6$  is by finding a mechanism whereby the population of  $^5I_6$  is depleted, effectively reducing the corresponding level lifetime and helping to maintain a population inversion. As mentioned before, there are two possible ways of depleting the population in level  $^5I_6$ :

- 1) pumping from  $^5I_6$  to some higher manifold, for example to  $^5S_2$ ;
- 2) lasing  $^5I_6$  to  $^5I_7$  at 2.96  $\mu\text{m}$ .

In the next set of calculations we have included the depletion of the  $^5I_6$  level. Everything else was left as in the previous model, except we again added pumping from the ground state. The depletion of the  $^5I_6$  level due to possible lasing from  $^5I_6$  to  $^5I_7$  at 2.9  $\mu\text{m}$  was taken into account by means of changing the effective lifetime of the  $^5I_6$  manifold.

The calculations for Ho:BYF showed that with 2 W of pump power at 750 nm and an effective lifetime of the  $^5I_6$  level reduced to 50  $\mu\text{sec}$  (due to lasing from  $^5I_6$  to  $^5I_7$ ) we achieve the following steady state populations: in  $^5I_7 \approx 9.4 \times 10^{19} \text{ cm}^{-3}$ , in  $^5I_6 \approx 2.1 \times 10^{20} \text{ cm}^{-3}$ , in  $^5I_5 \approx 1.39 \times 10^{20} \text{ cm}^{-3}$  (no inversion population yet between the  $^5I_5$  and  $^5I_6$  levels). But with 2 W of pump power at 750 nm and a 20  $\mu\text{sec}$  effective lifetime of the  $^5I_6$  level, the steady state populations calculated are the following: in  $^5I_7 \approx 9.97 \times 10^{19} \text{ cm}^{-3}$ , in  $^5I_6 \approx 1.42 \times 10^{20} \text{ cm}^{-3}$ , in  $^5I_5 \approx 1.48 \times 10^{20} \text{ cm}^{-3}$ , so there is population inversion between  $^5I_6$  and  $^5I_7$  ( $\approx 4.2 \times 10^{19} \text{ cm}^{-3}$ ), as well as between  $^5I_5$  and  $^5I_6$  ( $\approx 6 \times 10^{18} \text{ cm}^{-3}$ ). With a lower pump power of 1.6 W and a 10  $\mu\text{sec}$  effective lifetime of the  $^5I_6$  level, we have obtained the following steady state populations: in  $^5I_7 \approx 1.23 \times 10^{20} \text{ cm}^{-3}$ , in  $^5I_6 \approx 1.34 \times 10^{20} \text{ cm}^{-3}$ , in  $^5I_5 \approx 1.46 \times 10^{20} \text{ cm}^{-3}$ , and again there is population inversion between  $^5I_6$  and  $^5I_7$  ( $\approx 1.1 \times 10^{19} \text{ cm}^{-3}$ ), as well as between  $^5I_5$  and  $^5I_6$  ( $\approx 1.2 \times 10^{19} \text{ cm}^{-3}$ ).

With these population inversions ( $\Delta N \approx 10^{19} \text{ cm}^{-3}$ ) and typical cross sections ( $\sigma \approx 10^{-20} \text{ cm}^2$ ), the small signal gain coefficient,  $\gamma$ , is  $\approx 0.1 \text{ cm}^{-1}$ . If the length of the crystal is  $L = 3 \text{ mm}$ , then the small signal power gain is  $G = \exp(\Delta N \sigma L)$ . For a cavity with two mirrors having reflectivities  $R_1$  and  $R_2$ , the threshold for laser oscillation is determined by the requirement that the round-trip gain exceed one. If one considers only mirror losses, then the threshold condition is:

$$R_1 R_2 \exp(2 \Delta N \sigma L) \geq 1 \quad \text{or}$$

$$\gamma \geq \ln(1/R_1 R_2)/2L = \alpha$$

With a 99% reflectivity of both mirrors, the system is at three times threshold.

A more complete model would be desirable, preferably including additional high lying levels of the Ho ion. Such a fully upgraded version of the model would be useful in allowing more accurate comparison of energy transition rates and efficiencies as a function of power for pumping or lasing at different wavelengths either in a pulsed or in a cw mode. Such modifications and upgrades are rather substantial and can be carried out as part of an extended scope Phase II program.

### III. Material Growth and Fabrication

#### 3.1 Ho:BYF Growth and Fabrication

At the start of this project a number of Holmium doped YLF samples from boules grown by Dr. Jenssen for the previous SBIR project were made available to this work. The samples included Ho:YLF crystals with active ion concentrations of 1%, 2 %, 10% and 20 %. For this project two new Ho:BYF crystals were grown at CREOL under the supervision of Dr. H. Jenssen. The Ho<sup>3+</sup> concentration for these boules were 10% and 20%. Samples from a previously grown boule containing 2% holmium in BYF were also made available for comparison purposes.

The higher holmium concentrations were selected based on early calculations and previous results with Ho:YLF which indicated that higher concentrations are advantageous for pumping with 750 nm photons because cross relaxation processes become more significant as the concentration increases.

High quality feed material for growth were prepared from BaF<sub>2</sub>, Y<sub>2</sub>O<sub>3</sub> and Ho<sub>2</sub>O<sub>3</sub> by hydrofluorination utilizing anhydrous HF gas. These were used to grow the two new 10% and 20% crystals at CREOL using an available Czochralski growth station. Post-growth inspection of the boules determined they both had excellent purity. The boules were sufficiently large to allow slicing several reasonable size samples for further evaluations and tests. Laser quality rods of up to a few mm diameter and 1-2 in long could also be eventually fabricated from either boule. Several 2 mm samples were subsequently prepared from both boules for use in the spectroscopic measurements.

Several 2 mm sections from the 10% and 20% Ho:BYF boules were also sliced and delivered to Lasergenics where they were ground into seed rods to be used in the fiber growth experiments using the existing LHPG apparatus. These were oriented along the a-axis.

#### 3.2 Flouride Fiber Crystal Growth

We investigated the growth of Ho:YLF and Ho:BYF in fiber form. It is clear that the growth of crystal fibers of high melting point materials must overcome several difficult challenges in order to be useful for laser applications. Fluoride materials offer their own unique challenges primarily due to the high reactivity of fluorine, especially with oxygen. We will

describe the laser-heated pedestal-growth (LHPG) technique and give our results in this subsection.

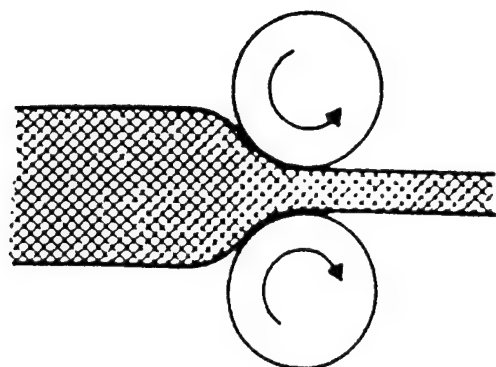
A number of techniques have been used to produce single crystal fibers and these are schematically illustrated in Figure 3.1.

In the hot rolling process, shown in Figure 3.1 (a), a rod is extruded through a series of progressively smaller wire dies to produce a fiber of reduced diameter.<sup>6</sup> The method is primarily applicable to relatively soft materials with low melting points, e.g. alkali halides.

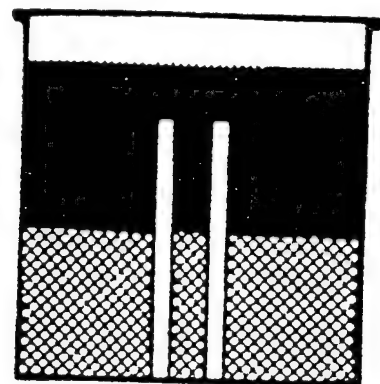
In the capillary-Bridgeman approach, Figure 3.1(b), a glass capillary tube is immersed in a melt of the crystal to be grown. The apparatus is slowly lowered through a temperature gradient to produce a crystalline core inside the glass tube.<sup>7</sup> Capillary-Bridgeman growth has primarily been applied to low-melting point organic crystals, as thermal expansion matching and chemical compatibility are critical requirements in this technique.

A number of techniques, for example the edge-defined film-fed growth and related processes, involve feeding the melt through a capillary to a die, which serves to shape the resulting fiber<sup>8</sup>, Figure 3.1(c). These methods are reviewed in reference 9. Single crystal fibers of silver and thallium halides have been produced by such techniques<sup>10,11</sup>, as have lower quality fibers of high melting point oxides such as sapphire, lithium niobate and spinel.<sup>51</sup> Particularly for high melting point materials, the choice of appropriate die material is crucial to minimize contamination of the melt and provide proper wetting conditions for stable growth. For sapphire growth with such a high melting point, this technique leads to in-diffusion of the die metal such as molybdenum.

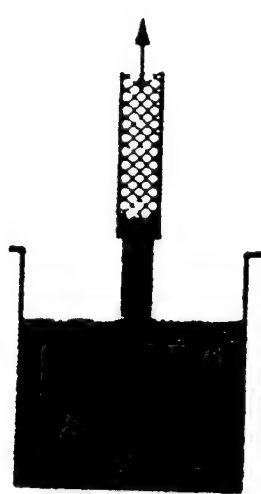
Laser-heated pedestal-growth, illustrated in Figure 3.1(d), uses a focussed laser beam to melt the tip of a solid rod of the material to be grown. A seed crystal is dipped into the melt, then withdrawn at a faster rate than the source rod is fed in, resulting in the growth of a fiber of reduced diameter. This approach has the advantages of eliminating any possibility of crucible contamination and of achieving melt temperatures limited only by the available laser power. Moreover, difficulties in the stabilization of the fiber diameter have in large part been solved. LHPG has been applied primarily to refractory oxide materials<sup>12-14</sup>, though halides,



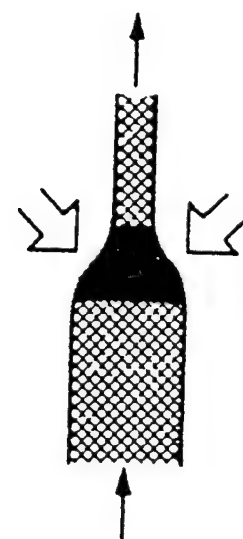
(a)



(b)



(c)



(d)

Figure 3.1. Techniques for the growth of single crystal fibers. (a) hot rolling; (b) Bridgeman growth in glass capillaries; (c) edge-defined film-fed growth; (d) laser-heated pedestal-growth (LHPG)

borides, and elemental semiconductors have also been grown.<sup>15</sup>

No one of these approaches is best suited to the production of high quality fibers in all materials.

As mentioned earlier, the LHPG technique involves melting the tip of a source rod with a focussed laser beam, dipping in an oriented seed crystal, then pulling a fiber while feeding in the source rod. This process, quite simple in principle, has several attractive features from a materials processing standpoint.

(1) Very high temperatures can be achieved, limited in principle only by the radiation temperature of the laser, and in practice by the available laser power. Only a few watts of absorbed laser power are necessary to raise the temperature of 500  $\mu\text{m}$  diameter rods of typical oxide materials to their melting point.

(2) The temperature gradients at the freezing interface are on the order of thousands of degrees per cm. These large temperature gradients, in turn, allow stable growth at rates orders of magnitude larger than in bulk crystals, typically 0.1-20mm/min. As thermal stresses in a surface cooled cylinder scale with the radius, these large gradients do not lead to a cracking problem in small diameter fibers.

(3) The process is entirely crucibleless, minimizing the incorporation of undesired dopants, and facilitating the growth of a variety of materials in the same apparatus with a high degree of purity equal to the purity of the starting material. (4) It is theoretically predicted that in the absence of phase separation or volatilization, the composition of the source rod and the fiber should be identical, so that the effective distribution coefficient approaches unity<sup>15-17</sup>, which is particularly important in the growth of compositionally uniform solid-solution crystals. The prediction that convection in the molten zone is not oscillatory further reduces the probability of compositional striations.

In order to take advantage of these features of the LHPG process to produce fibers of high melting point materials, stable growth conditions must be realized, which in turn requires thermal and mechanical stability of the growth zone, and symmetric heat input from the laser. The heat should be delivered to a spot whose size is comparable to the source rod diameter, to produce the short molten zones necessary for stable growth. The apparatus designed to meet these requirements is now described.

A block diagram of our fiber growth apparatus is shown in Figure 3.2. A focused CO<sub>2</sub> laser melts a surface tension supported liquid zone which bridges the source and seed rods. Growth proceeds by simultaneous upward translation of the seed and source rods with the molten zone positioned between them. The laser focal spot, and consequently the molten zone, remain fixed during fiber growth. The source rod to fiber diameter ratio is set by mass conservation to be the square root of the fiber to source rod translation rate.

In order to achieve a constant fiber diameter, stable fiber growth conditions must be realized. This in turn dictates a rigid mechanical apparatus, smooth source feed and fiber pull rates, stable laser power, and symmetric heat input into the molten zone. The LHPG apparatus utilizes novel optical and mechanical systems to achieve stable growth conditions and a uniform diameter fiber. Descriptions of the fiber growth apparatus sub-systems are given below.

A polarized CO<sub>2</sub> laser serves as the heat source for crystal growth. The water cooled laser cavity is temperature stabilized and produces a polarized HE<sub>11</sub> output mode with power fluctuations of less than 0.75%. A polarization power control system is used to adjust the laser power incident on the molten zone. After passing through a ZnSe beam expanding telescope and some beam steering optics the CO<sub>2</sub> beam enters the controlled atmosphere growth chamber.

Within the growth chamber a novel optical system focuses the laser beam onto the fiber with a 360 degree axially symmetric distribution as shown in Figure 3.3. The symmetric irradiance prevents cold spots in the growth zone and represents a significant improvement over the previously used two beam,<sup>18</sup> rotating periscope,<sup>19</sup> or ellipsoidal<sup>20</sup> focusing systems.

A novel optical element incorporated into the design is a reflexicon<sup>21</sup> which consists of an inner cone surrounded by a larger coaxial cone. In order to achieve good optical performance it is critical that the reflexicon's two cones be accurately aligned. A mated surface design using diamond turned copper optical components, assures centering of the cone's axes. A gold coating on the copper optical surfaces enhances reflectivity and protects

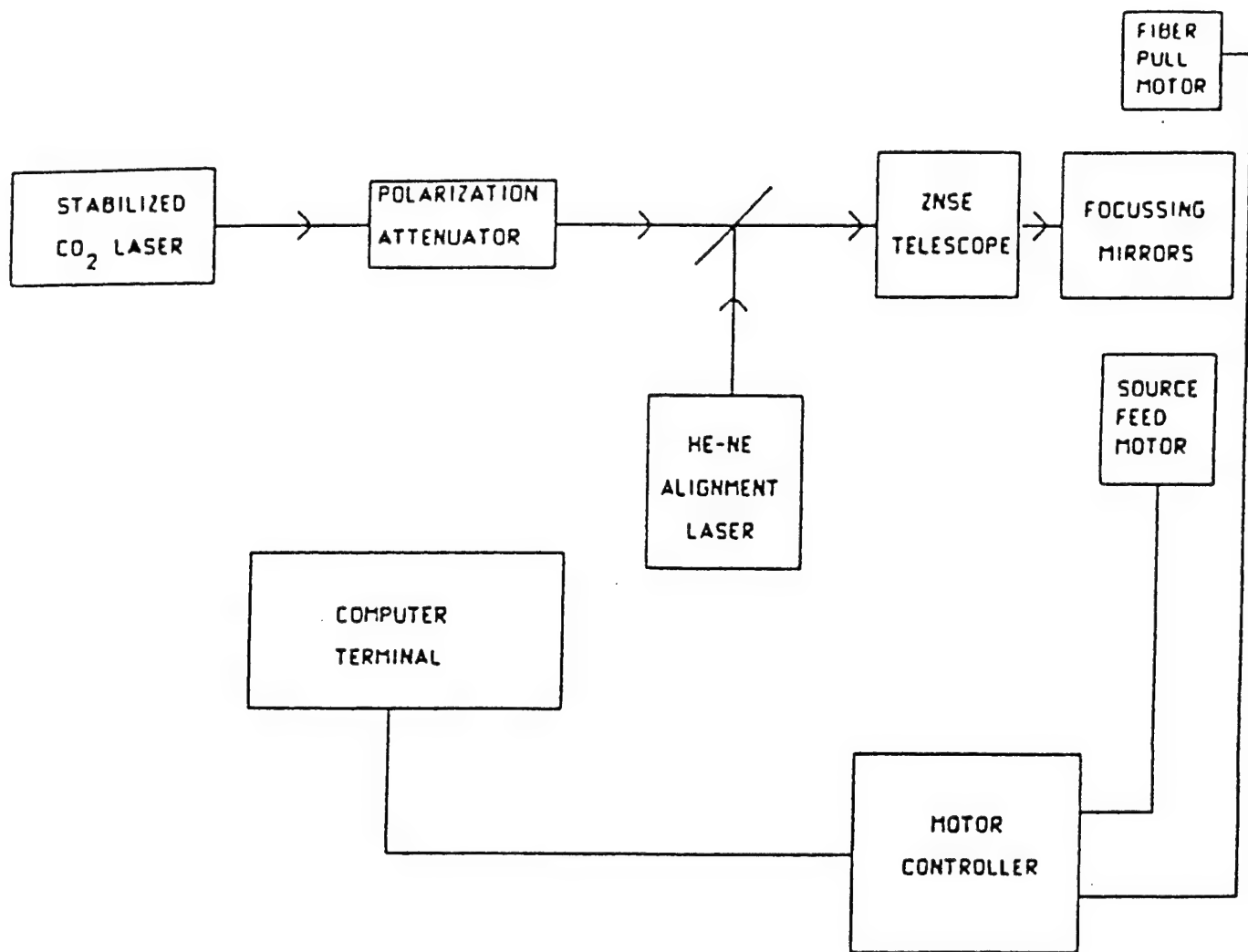


Figure 3.2. Block diagram of the LHPG apparatus.

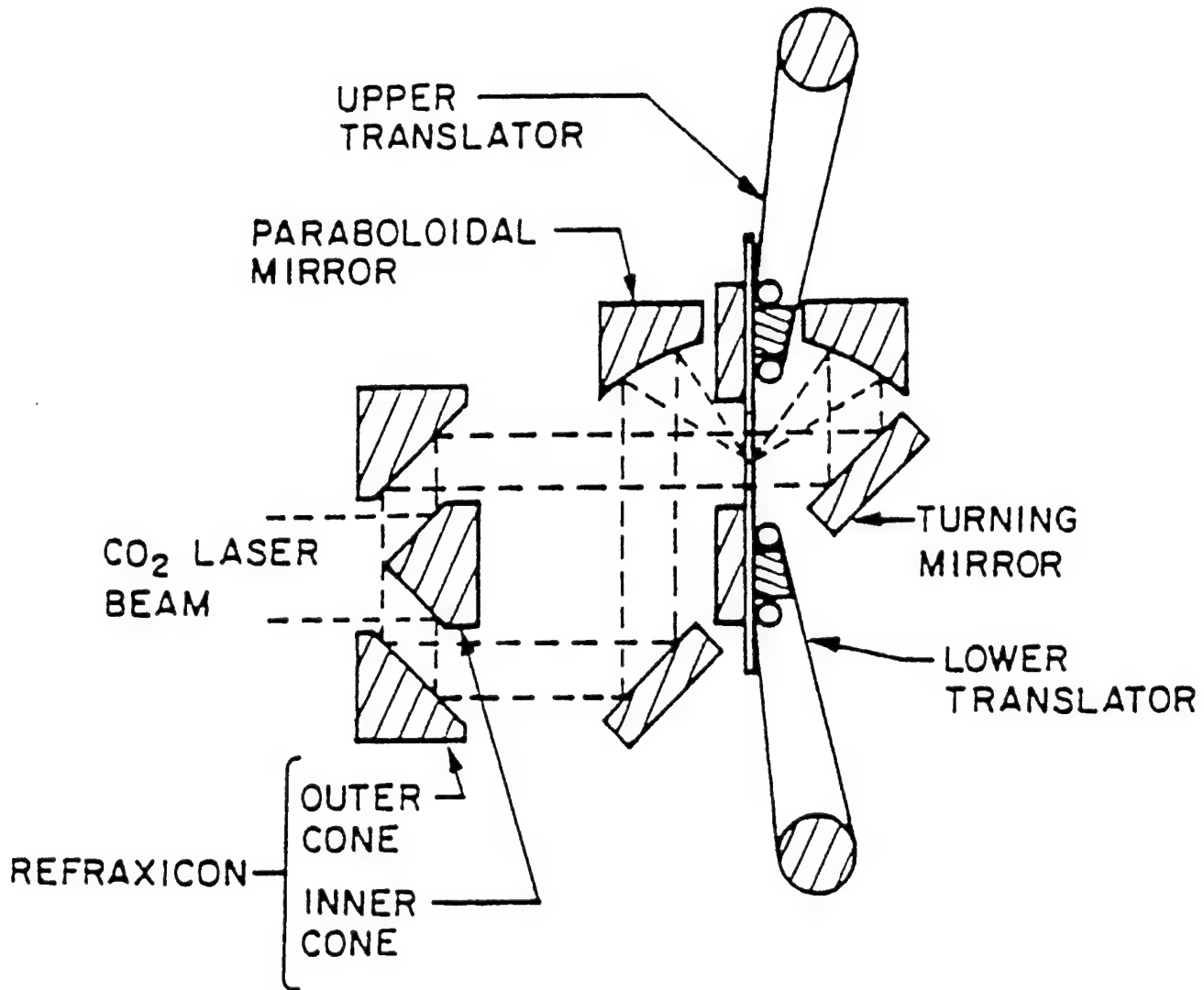


Figure 3.3. Cross-section of the growth head, showing the reflexicon focussing system and the fiber translation mechanisms. The optical elements are rotationally symmetric about their centerline.

the copper substrate. The reflexicon and parabolic mirror provide near diffraction limited f/2 focusing, yielding a minimum spot size of 30 microns. This tight focus is important for the stable growth of small diameter fibers. The focal spot size can be controlled by modifying the input beam divergence with the focusing telescope. X-Y stages on the fiber and source rod translation devices permit adjustment of the fiber position with respect to the fixed laser focal spot.

Fiber translation speed is controlled by a phase-locked control circuit which enables d.c. motor operation over a 250,000:1 speed range with acquisition times of 1 ms. A useful control option allows the pull-to-feed translation ratio to be fixed while adjusting the growth speed. Since starting transients exist during initiation of fiber growth, a slow growth rate allows time for adjustments. As the equilibrium growth conditions are reached, the growth speed can be increased without affecting the fiber diameter.

The first step in the growth of a fiber is the preparation of the source material. The requirements on the source rod are: (1) it should have the composition of the desired end product (assuming that no volatilization takes place during growth); (2) it should have constant density, and have as close to theoretical density as possible; (3) the cross-section should be constant, as small as possible, and preferably circular. We have had good success using a centerless grinder to fabricate starting rods with diameters as small as 300  $\mu\text{m}$  and tapers as small as 1  $\mu\text{m}/\text{cm}$ . The rod material itself can be a single crystal obtained elsewhere, a polycrystalline source material from solidified melts, a cold-pressed and sintered powder, or a hot-pressed powder. All of these have been used successfully.<sup>22-24</sup>

The next step in the growth is to melt the tip of the source rod with the CO<sub>2</sub> laser beam, and to dip in a seed crystal. The seed can be an oriented centerless-ground rod, a previously grown fiber or, in the case of a first growth, a platinum wire or a fiber of a higher melting point material. Because of the symmetrical heat input of the reflexicon focussing system, the azimuthal orientation of the seed has no direct effect on the growth.

After the seed is oriented, the laser power is adjusted to produce the desired length of molten zone. The molten zone must also be adjusted to produce the proper contact angle between the melt and the seed.

Growth is initiated at this point by simply simultaneously switching on the pull and feed motors, which have previously been set to run at the appropriate speeds. Lengths over 100 cm have been grown to date. In principle, lengths of fiber are limited only by the available feed material. This latter limitation is not serious in practice, in that each centimeter length of 1.25 mm diameter feed material could produce 5 meters of 50  $\mu\text{m}$  diameter fiber if processed three times.

Only a modest amount of power is necessary to produce an appropriate molten zone. For example, 2 watts incident power is adequate for the growth of a 170 $\mu\text{m}$  diameter sapphire fiber from a 500 $\mu\text{m}$  diameter source rod. Typical growth rates are 0.1-20 mm/min, several orders of magnitude faster than is typical of bulk crystal growth. The mechanism that limits the maximum possible growth rate appears to vary for different materials. In Reference 66, Nightingale shows that for sapphire grown at rates faster than 8 mm/min, constitutional supercooling with respect to an unknown species, possibly Al or O<sub>2</sub> leads to the formation of microvoids along the axis of the fiber that cause severe optical scattering problems. Growth in a He atmosphere to increase the thermal gradients at the interface may lead to higher useful growth rates.

We have generally found it possible to grow fibers approximately a factor of three smaller in diameter than the source rod for growth in air. As the diameter reduction is increased, the damping coefficient for diameter variation decreases, eventually becoming negative at a critical diameter reduction  $R_c$ . Growth at diameter reductions larger than  $R_c$  is thus unstable. For Al<sub>2</sub>O<sub>3</sub> this instability occurs at a reduction between 3 and 4 when grown in air. It is possible that diameter reductions between 4 and 5 could be achieved when grown in a helium atmosphere.

The LHPG technique is an excellent method to grow single crystal fibers. It is likely that for many high melting point materials no other technique will be able to grow similarly good quality single crystal fibers. With this process, the atmosphere can be accurately controlled during growth as well as the crystal growth temperature. Because of the steep thermal gradients in the growth zone with this technique, the crystal structure that is "frozen in" can to some degree be controlled. We feel that this is an ideal technique to investigate the growth of high melting point materials such as Ho:YLF and Ho:BYF. This technique is closely related to the float-zone method which is

the best known technique to grow incongruently melting compositions.

The Ho:YLF and Ho:BYF source material and seed crystals were obtained from Dr. Hans Jenssen which were single crystal material grown by him. We fabricated both materials into rods that were 1 mm x 1 mm in cross section and several centimeters in length. The source rods and seed rods were mounted in alumina tubes with high temperature cement. The seed rods were a-axis aligned so the growth direction was along the a-axis.

After discussions with Dr. Jenssen, we decided to try growing Ho:YLF using a flowing gas atmosphere of pure nitrogen. Although we were aware that the fluorides were highly reactive with oxygen, we felt that with the LHPG technique, because of the rapidness of the growth process, the melt material would only be subjected to the atmosphere for a short time. The melt zone is only approximately 0.5 mm long. The growth speeds were from 1 mm/min to about 6 mm/min so that the exposure time would be from 5 to 30 seconds. This is long enough to react at the surface but if the oxygen concentration is low enough the interior of the fiber should be reaction-free. It is difficult to say what the oxygen concentration will be with our flowing gas method but because of the simplicity of the technique we felt it would be worth trying. The power needed to melt the source rod was quite low and we found it to be necessary to cut back the laser power to less than 10 W. Even though the melt zone was quite turbulent. It appeared that the material was melting incongruently. We could observe clumps breaking away from the source rod and rise into the melt and disappear as they melted. Turbulence could also be observed at times around the fiber freezing zone. This is much more unstable than we like to see for good quality fiber growth. We were able to grow fibers of the material but the fiber diameter fluctuations were too great for good quality fibers because of the instability of the melt zone. Many growth runs were made in an attempt to find the optimum laser power and fiber pull speeds but we were not able to obtain a good quality fiber of Ho:YLF. We next tried the Ho:BYF material because the melt temperatures and other characteristics are different from those of Ho:YLF. However, similar problems arose with this material as well. Short sections of both types of fibers that we grew were sent to Dr. Jenssen's laboratory for analysis. It was determined that the oxygen content of the fibers was much to high, nearly 30% of the fiber material was  $\text{Y}_2\text{O}_3$ . It was clear then that too much of the material was reacting so that we had to remove a much greater fraction of oxygen from the growth chamber, that the flowing nitrogen would not dilute the oxygen to the needed levels. Moreover, we needed to consider the fact that the material in both cases was melting incongruently.

First we addressed the oxygen problem. Several modifications were made to the chamber in order that we could feel confident that we were able to get the oxygen concentration to less than one part per million. Several improvements were made to the pumping system and the chamber to achieve this. The vacuum chamber was then tested and the leak rate measured to be less than 25 ml/hr. As a typical growth run lasts less than 2 hours after back-filling with nitrogen gas having an oxygen purity of better than  $0.5 \times 10^{-6}$  parts oxygen, by the end of the run the oxygen concentration could be as high as  $2 \times 10^{-4}$  parts. During several growth runs of both materials, Ho:YLF and Ho:BYF, we found that the melt zone was more stable but still the fiber diameter fluctuations were too large.

We next attempted to address the issue of the incongruent melting of the melt zone. We first considered the loss of lithium in the melt zone during the growth of Ho:YLF. We seeded the tip of the source with LiCO<sub>3</sub>. Quite different melting characteristics were observed so we felt this to be a promising approach although power optimization needed to be done. A flux of LiF was tried next, again with Ho:YLF. Again, much more stable growth was observed. A section of this fiber was sent to CREOL for analysis and showed much less oxygen content but the other parameters need to be optimized in order to improve the optical quality. These were not of laser quality. On these runs both nitrogen and argon were tested as flushing gases. Little differences were noted between the two gases.

We next tried the LiF flux for the growth of Ho:BYF as this material has better congruency than Ho:YLF. Unfortunately we did not have enough time to develop the optimum laser power and pulling speeds with this material. Clearly, more work needs to be done to optimize the growth parameters for both Ho:YLF and Ho:BYF. We need to make further improvements to reduce further the oxygen concentration in the growth chamber and we need to further optimize the flux concentration in the melt. We believe that there was some lithium and fluorine loss from the melt during growth so that it may be necessary to incorporate LiF in the source rod for the growth of Ho:YLF or coat the source rod for this material. Ho:BYF may prove the easier material because it is much closer to congruency than Ho:YLF. A great deal was learned about the growth of these two materials during the course of this program. We are confident that with further reduction in the oxygen content and with the optimization of the flux concentration we will be able to grow laser quality Ho:YLF and Ho:BYF fibers.

content and with the optimization of the flux concentration we will be able to grow laser quality Ho:YLF and Ho:BYF fibers.

## IV. Experimental Studies

### 4.1 Spectroscopic Evaluations

Spectroscopic measurements were performed to help determine the position of the Ho<sup>3+</sup> energy levels as well as the relative strength of key absorption, emission and cross-relaxation processes under pumping at specific wavelengths. Spectroscopic measurements were conducted at CREOL's facilities using available equipment, sometimes modified for this project. Throughout the measurements, particular emphasis was placed on characteristics of those absorption and emission transitions that may impact the 4  $\mu\text{m}$  line of interest.

The experiments were carried out on several existing Ho:YLF samples of varying concentrations from a low of 1% to a high of 20%, and on samples of Ho:BYF grown for this project, as discussed in the previous section.

#### 4.1.1 Absorption Spectra

Absorption measurements were conducted using a Perkin-Elmer Lambda 9 Spectrophotometer. This instrument consists of a dual beam comparator device with the signal taken to be the ratio of intensities of the sampling to the reference beam. Polarized measurements were made by placing a matched set of Glan-Thompson polarizers in the sample and reference beam. The data scans were controlled and stored with a PC compatible computer. The spectral resolution for all the measurements was generally set to 0.5 nm.

Absorption spectra were used to determine the cross sections of transitions from the ground state to various upper levels. Absorption scans were made covering the wavelength range from the UV into the IR. As an example, the absorption spectrum is shown in Figure 4.1 for the 10% Ho:BYF sample. Figure 4.2 gives detail of the 750 nm absorption line for the same sample. Similar scans are available for the 20% Ho:BYF sample as well as for the various Ho:YLF samples. As the relative absorption intensities in Figure 4.1 show, the 750 nm absorption line from the ground state is rather weak. In fact, it could only be measured for the higher concentration samples.

Results for some key absorption coefficients,  $\alpha$ , and cross sections,  $\sigma$ , derived from the full set of absorption data were as follows:

Absorption spectrum of 10% Ho:BYF (random polarization)

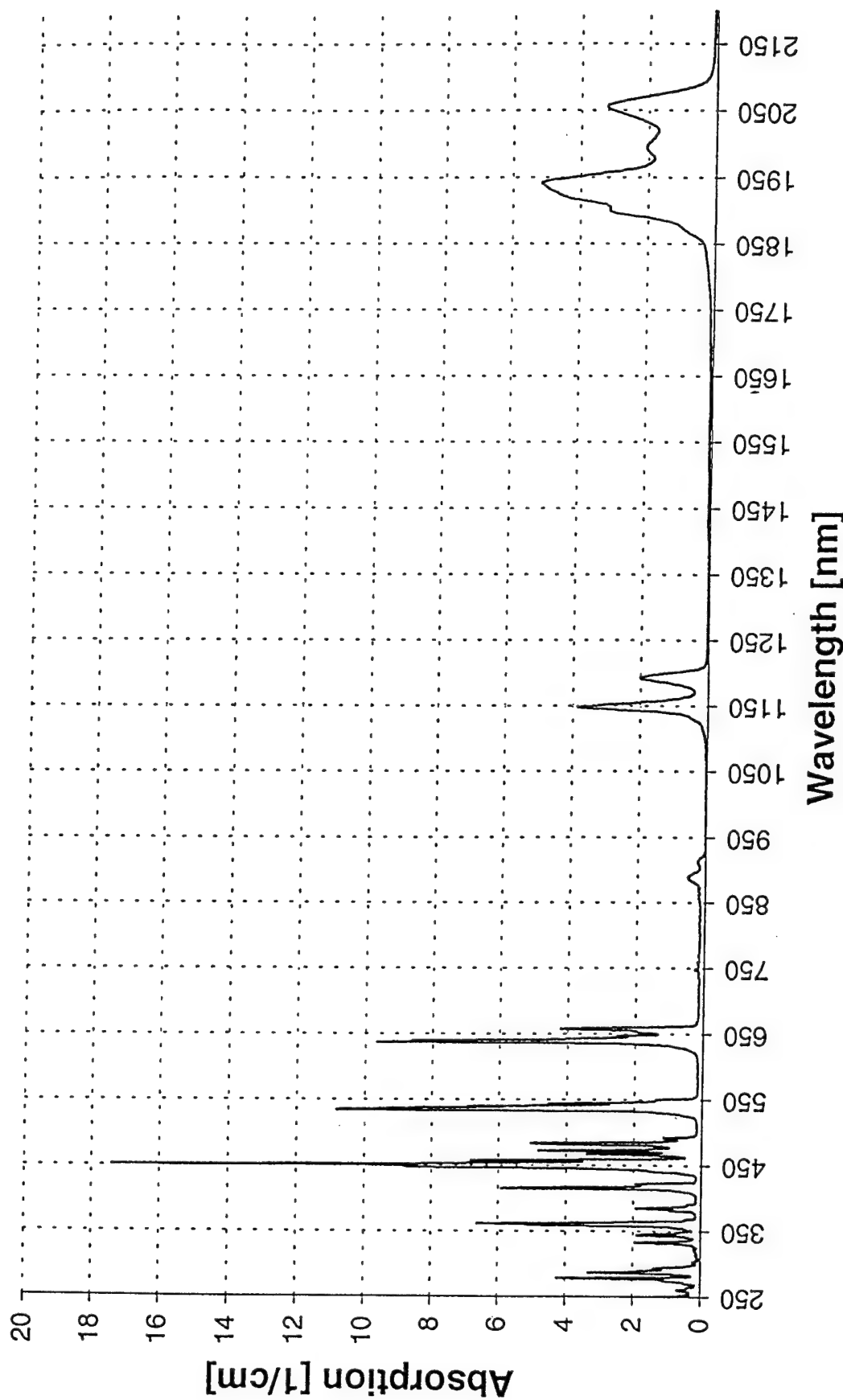
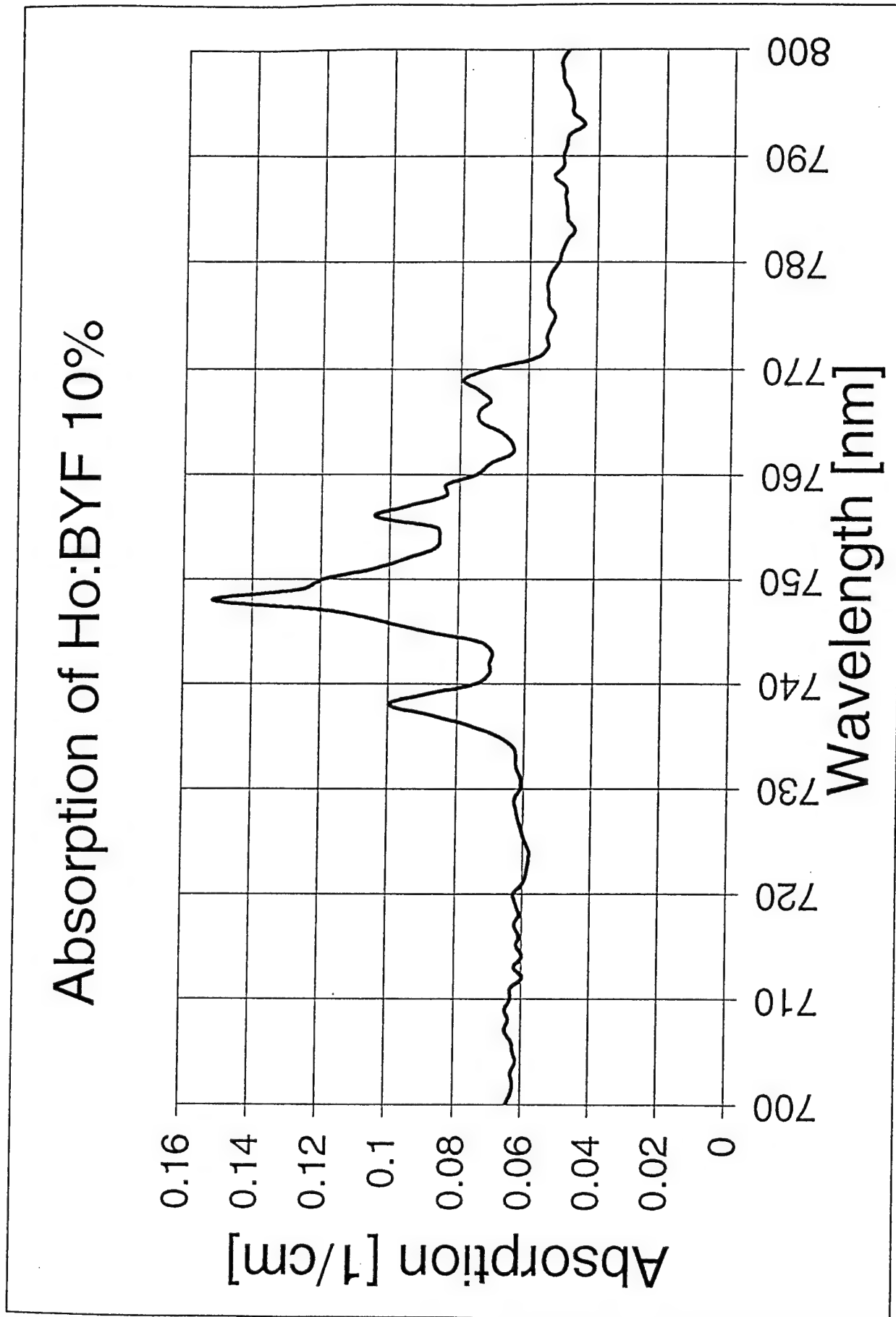


Figure 4.1



<u>Transition</u>	<u><math>\lambda</math> (nm)</u>	<u><math>\alpha</math> (cm<math>^{-1}</math>)</u>	<u><math>\sigma</math> (cm<math>^2</math>)</u>
$^5I_8 \Rightarrow ^5I_4$	750	0.104	$8 \times 10^{-23}$
$^5I_8 \Rightarrow ^5I_5$	900	1.078	$8.3 \times 10^{-22}$
$^5I_8 \Rightarrow ^5I_6$	1150	6.9	$2.65 \times 10^{-21}$
$^5I_8 \Rightarrow ^5I_7$	1950	11.51	$4.42 \times 10^{-21}$

The measurements could also be used to derive information about absorption coefficients and cross sections for the visible absorption lines, but these were not addressed in detail on this project.

#### 4.1.2 Fluorescence Emission and Excitation Spectra

To determine the relative positions of the energy levels of interest in Ho:BYF, detailed fluorescence and excitation spectral measurements were made. These data were used to derive magnitudes of several relevant stimulated emission cross sections.

A double SPEX spectrofluorimeter was used in the fluorescence emission and excitation spectrum measurements. This instrument has two double-grating monochromators in the excitation and emission channels. The radiation source is a Xenon arc lamp. An excitation spectrometer filters the light from the lamp to select particular wavelengths. Emitted radiation is filtered by an emission spectrometer feeding the signal to a detector photomultiplier (PMT). Scanning the emission spectrometer with a stationary excitation wavelength produces a spectrum of radiation emitted by the sample. Scanning the excitation spectrometer at a constant emission wavelength yields the excitation spectrum. Signals from the PMT are amplified with a lock-in amplifier and directed to a data acquisition system. A Labview program controls both the input and output channels of the automated data acquisition system.

Figure 4.3 shows the fluorescence emission spectra for low (1%) and medium (10%) concentration Ho:BYF, under pumping at 455 nm. The emission intensities at 10% were scaled to match the 1% data at the 660 nm emission peak. Figure 4.4 shows the fluorescence emission spectrum taken for the 10% Ho:YLF under the same 455 nm pumping conditions and Figure 4.5 shows similar data for a 20% Ho:YLF sample. With this blue excitation wavelength,

## Emission Spectra of 1% & 10% Ho:BYF (random polarization)

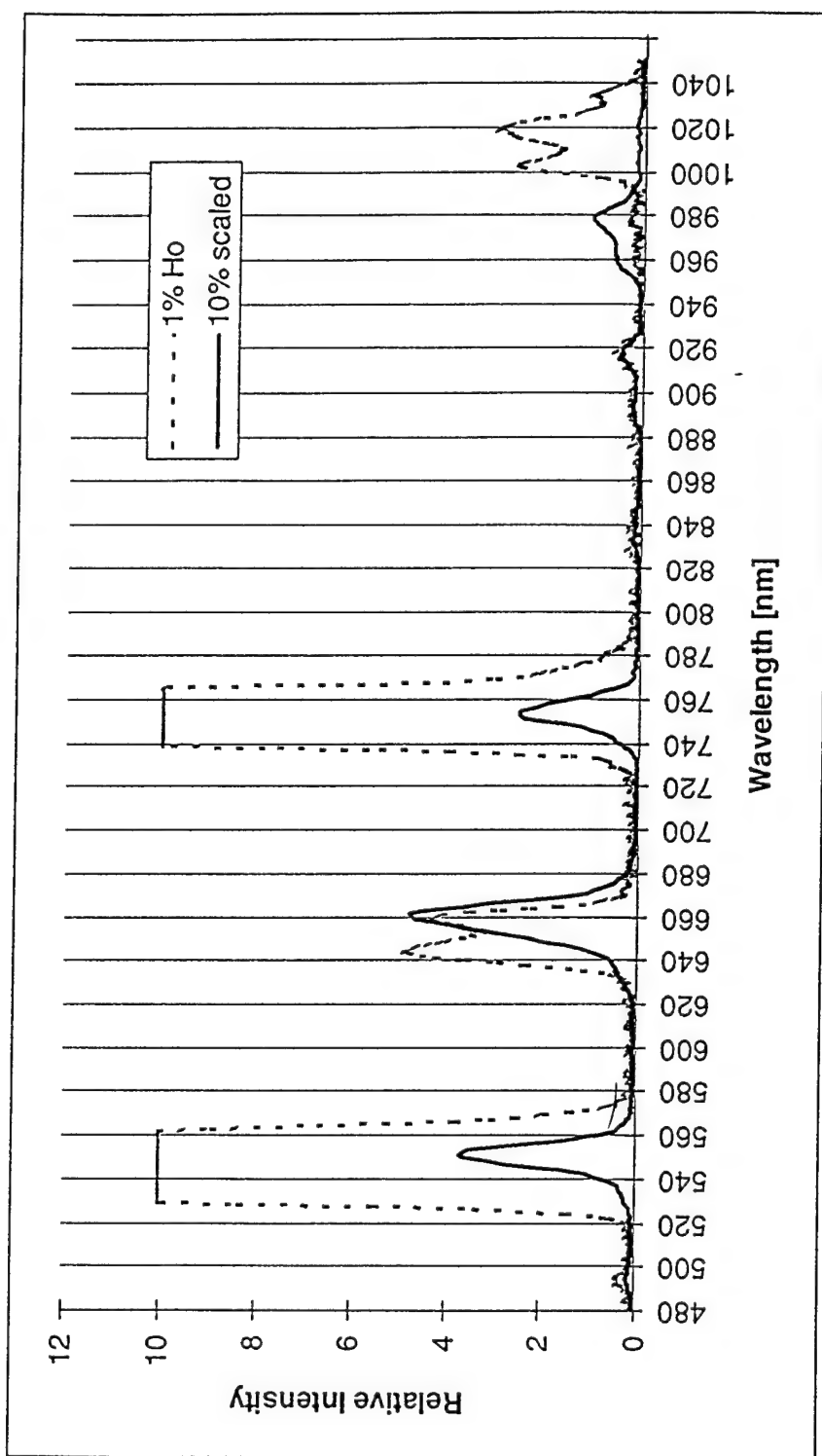


Figure 4.3

Emission Spectrum of YLF:Ho 10 % at Pump  
Wavelength 455 nm (random polarization)

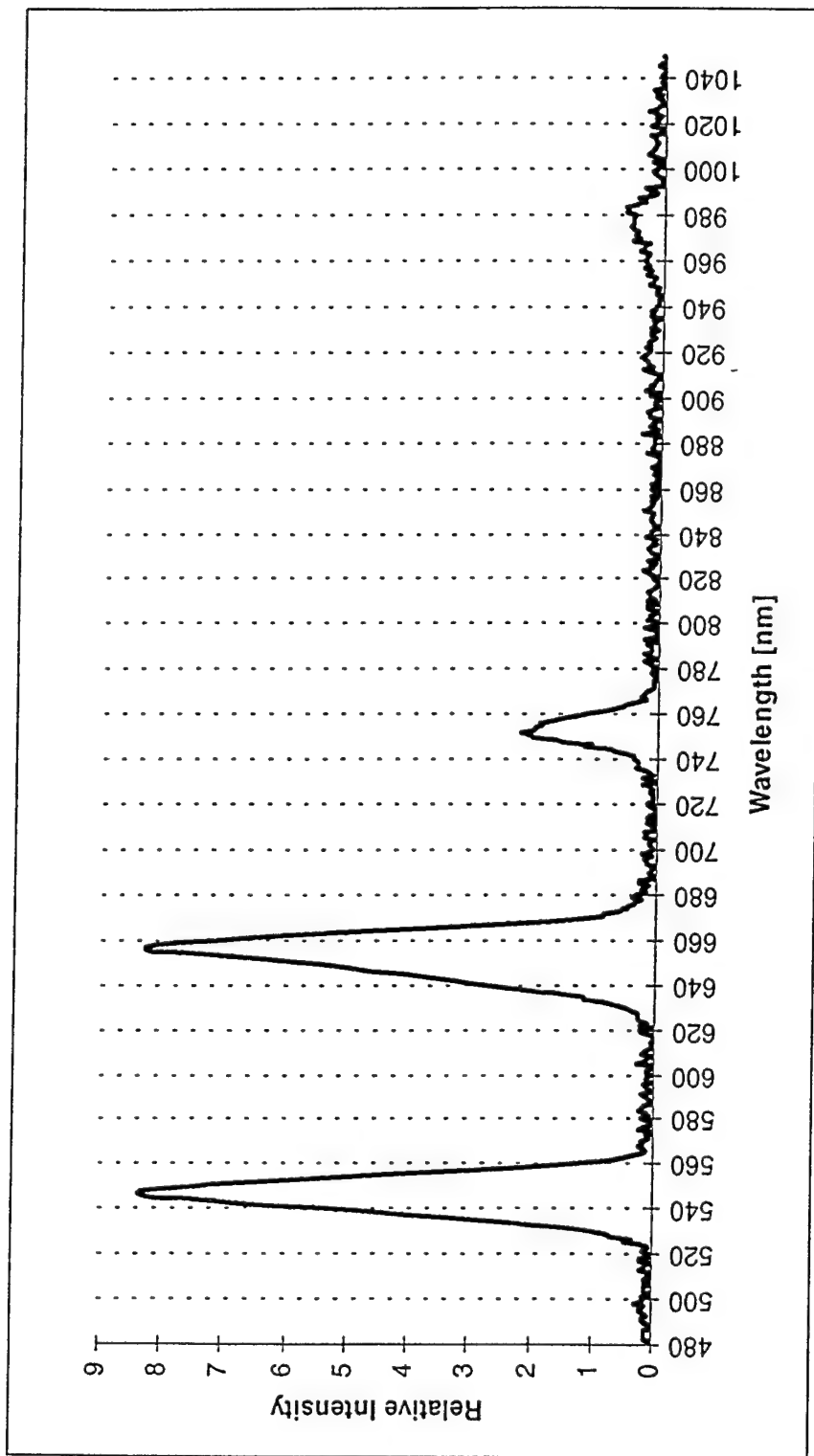


Figure 4.4

Emission Spectrum of YLF:Ho 20 % at Pump  
Wavelength 455 nm (random polarization)

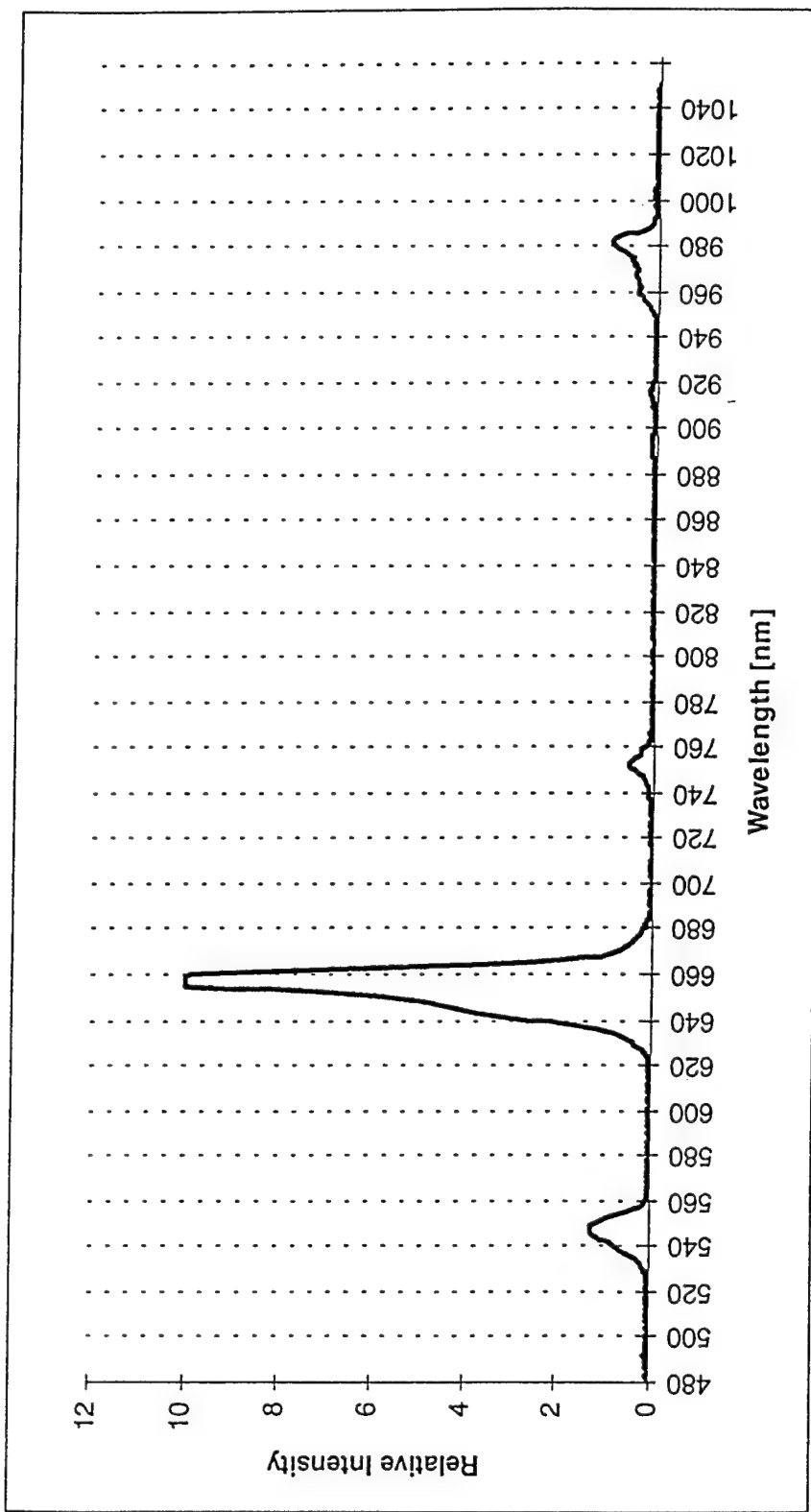


Figure 4.5

photons are pumped from the  $^5I_8$  ground state to the high lying  $^5G_6$  level. This level can immediately relax to the  $^5S_2$  ( $^5F_4$ ) level, or it can undergo a cross relaxation process to the  $^5F_5$  level. Figure 4.3 indicates three intense fluorescence lines at 546, 750 and 1020 nm originating from the  $^5S_2$  level in the 1% Ho:BYF sample. These represent transitions to the  $^5I_8$ ,  $^5I_7$  and  $^5I_6$ , respectively. Verification of  $^5S_2$  as the originating level for all three lines was provided by lifetimes measurements (see below) which were the same for all three transitions. These emissions are significantly reduced in the 10% sample, which could be attributed to a cross relaxation process taking place. The strong emissions at 660 nm (attributed to  $^5F_5 \Rightarrow ^5I_8$  decay) and 980 nm (due to  $^5F_5 \Rightarrow ^5I_7$ ) are evidence of relaxation processes from either  $^5S_2$  or  $^5G_6$  to  $^5F_5$ . (similar fluorescence decay lifetimes measured for the 659 and 981 nm transitions, confirmed that they both originate on the same  $^5F_5$  level). The contribution of these relaxation processes appears to increase with concentration, as shown by the difference between the 1% and 10% emission spectra for Ho:BYF. In particular we note the striking reduction in emission intensity at the 1020 nm line going from the 1% to the 10% sample and the corresponding increase in 980 nm emission from  $^5F_5$ .

A similar trend is shown by the emission spectra of Ho:YLF. For example, Figure 4.3 for the 10% Ho:YLF sample has emission spectra similar to the 10% Ho:BYF of Figure 4.4 including the near absence of emission at the 1020 nm line, the appearance of emission at 980 nm and comparable emission intensities for the 546 nm ( $^5S_2 \Rightarrow ^5I_8$ ) and 659 nm ( $^5F_5 \Rightarrow ^5I_8$ ) lines. The trend continues for the 20% Ho:YLF samples shown in Figure 4.5, where a marked increase in the relative intensity of emission from  $^5F_5$  at 659 nm is seen over emissions from the  $^5S_2$  level (at either 546, 750, or 1020 nm), indicating the further increase in the contribution from cross relaxation processes to the  $^5F_5$  level.

Thus, pumping to  $^5G_6$  in the higher concentration material results in cross relaxation to the  $^5F_5$  level as a dominant decay mechanism, largely bypassing the  $^5S_2$  level, in both Ho:BYF and Ho:YLF. This is particularly well corroborated by the appearance of emission at 981 nm (attributed to the  $^5F_5 \Rightarrow ^5I_7$  transition) at higher concentrations, at the expense of the 1020 nm emission (from  $^5S_2 \Rightarrow ^5I_6$ ) which nearly disappears in the 10% concentration materials.

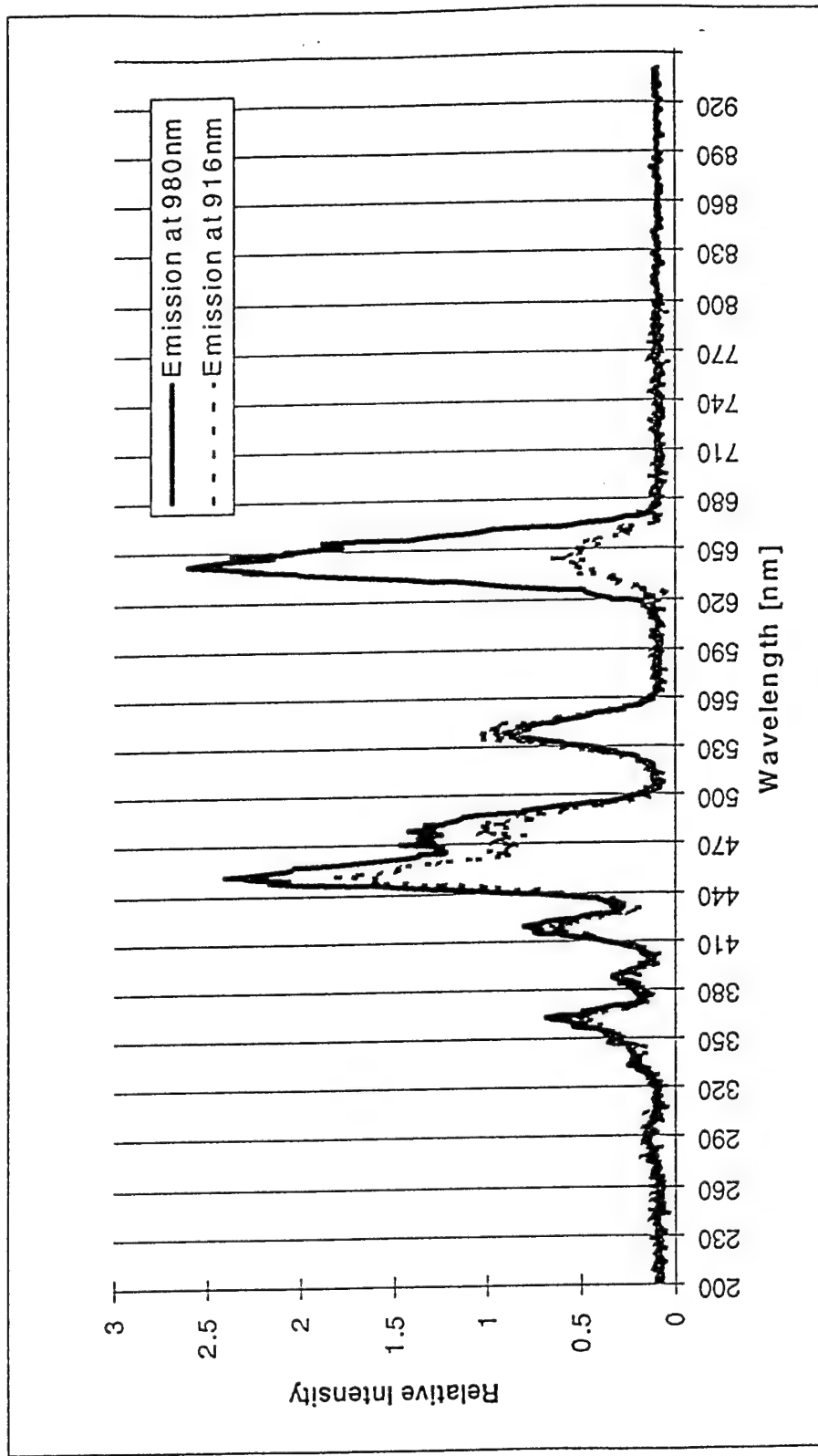
As one other item of interest we note the relative weakness of the transition at 915 nm (attributed to the  $^5I_5 \Rightarrow ^5I_8$  decay) in all the samples. This could be indicative of the weakness of the  $^5F_5 \Rightarrow ^5I_5$  transition (radiative at 2.37 nm). For Ho:BYF the ratio of relative emission intensities

at 660 to that at 915 nm is nearly the same for the two concentrations of Ho:BYF (Figure 4.3). For the Ho:YLF samples the relative intensity ratio for these two lines appears to increase as the concentration increases from 10% to 20% (Figures 4.4 and 4.5). Unfortunately data were not available from the 1% Ho:YLF sample to confirm this trend. Also the data for the 915 nm line points to the need to obtain more detailed emission measurements using pumping at 546 nm (to the  $^5S_2$  level) so as to elucidate the relative strength of the upper level transitions and cross relaxation processes that can feed the  $^5I_5$  level in both holmium doped materials.

Some clues to the fundamental differences between YLF and BYF are provided by excitation spectra taken for the two materials. For example Figure 4.6 shows the relative contributions to emission in 10% Ho:YLF from  $^5F_5$  and  $^5I_5$  (represented by respective transitions at 981 and 915) following absorption to several different levels including the  $^5G_6$  multiplet (450-490 nm),  $^5S_2$  (540 nm) and  $^5F_5$  (640 nm). This figure shows that emission from  $^5F_5$  (corresponding to 980 nm) is triggered primarily by absorption to  $^5G_6$  and  $^5F_5$  and to a lesser extent to  $^5S_2$ . However, the role of the  $^5F_5$  level in producing emission from  $^5I_5$  (at 915 nm) is diminished compared to that of  $^5S_2$ . As concentration increases, the role of  $^5S_2$  absorption in contributing to  $^5I_5$  emission becomes more important, as can be seen from a comparison of the peaks at 660 nm and 546 nm in Figure 4.7 and Figure 4.8, both for a 20% Ho:YLF sample. The significant feature to note is that, at this higher concentration, the high degree of correlation of  $^5S_2$  absorption from the ground state (at 546 nm) to  $^5I_5$  emission (at 915 nm) is similar to that of the 10% sample (see figure 4.6) as is the lower correlation between  $^5S_2$  absorption from the ground state to emission from  $^5F_5$  (at 981 nm).

These measurements may indicate that, in Ho:YLF, a strong cross relaxation process exists between levels in the upper  $^5G_6$  multiplet and the  $^5F_5$  level, with the latter exhibiting only weak transition to  $^5I_5$ . This cross relaxation process bypasses the  $^5S_2$  level, which does contribute to  $^5I_5$  through another cross relaxation process between  $^5S_2$  and  $^5I_4$ . Alternatively, the radiative 1.4  $\mu\text{m}$  transition from  $^5S_2$  can also populate the  $^5I_5$  level and is most effective at lower concentrations, where cross relaxations are less significant. Thus, while there are two paths to increase the  $^5I_5$  population starting at  $^5S_2$ , there do not appear to be similarly attractive transitions from  $^5F_5$ , in either low or high concentrations, at least in Ho:YLF. Therefore, excitation to the  $^5G_6$  level will be increasingly less effective in triggering the 4  $\mu\text{m}$  transition as the concentration increases. Clearly, even if there was a three photon transition at 750 nm (ending at  $^5G_6$ ), this may not necessarily be advantageous to producing the desired inversion, especially at the higher (20%) concentrations. We note that this is not an issue under

# Excitation Spectra of YLF:Ho 10% at Two Different Emission Wavelengths (random polarization)



Excitation Spectrum of YLF:Ho 20% at Emission  
Wavelength 915nm (random polarization)

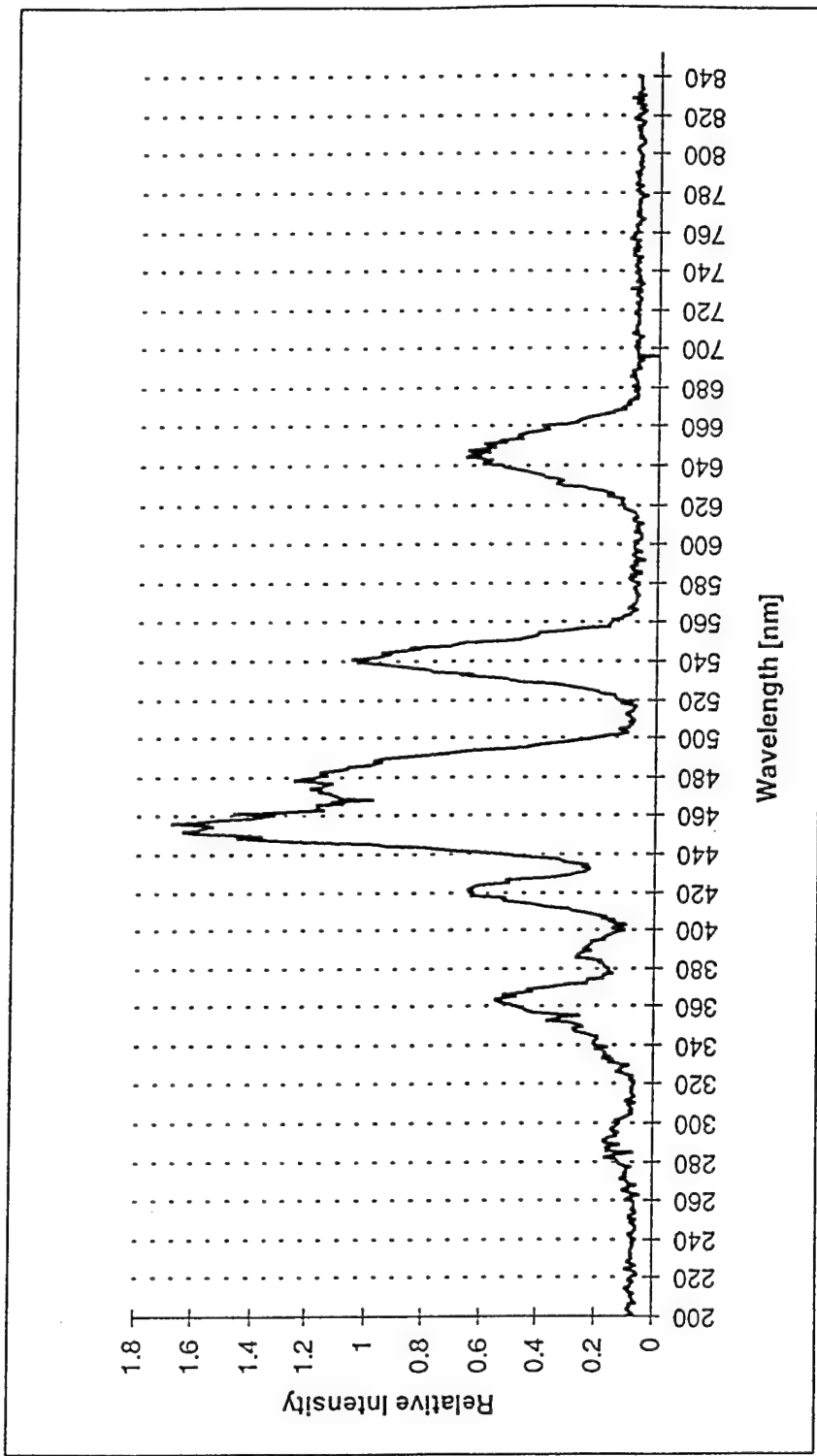


Figure 4.7

# Excitation Spectrum of YLF:Ho 20% at Emission Wavelength 981nm (random polarization)

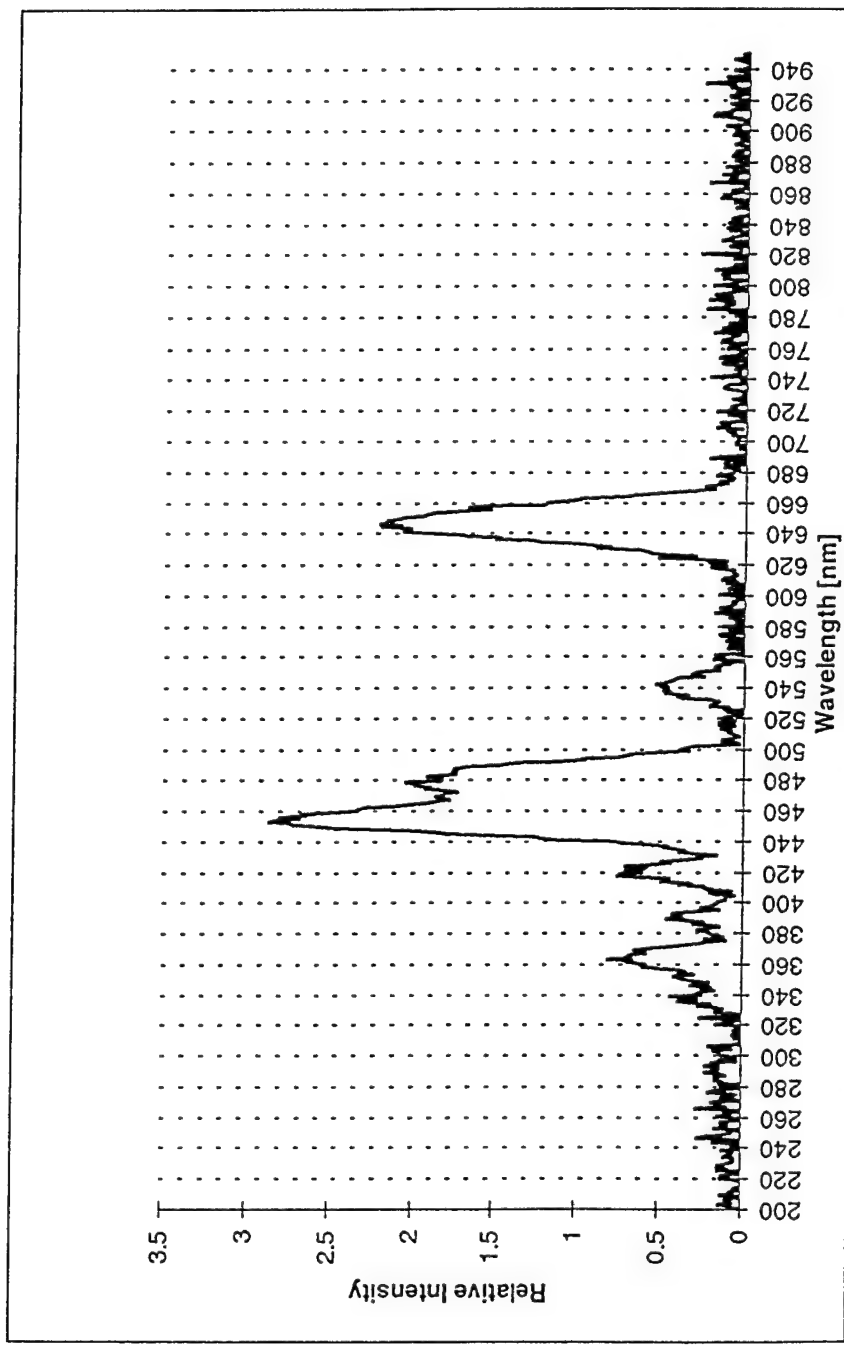


Figure 4.8

conditions of excitation to  $^5S_2$  (through, e.g., a two-photon absorption) since the  $^5F_5$  will not play a significant role in this case.

Based on indications available thus far, the situation may be different for Ho:BYF. Excitation spectra for this material (not shown) indicate a possibly stronger transition channel between  $^5F_5$  and  $^5I_5$ , with the  $^5S_2$  level playing a smaller role as compared to Ho:YLF, even at higher concentrations. Therefore, if there was a way to provide excitation to  $^5G_6$  (e.g., by a three-photon absorption at 750 nm or by some combination of absorption and an upconversion process), cross relaxation processes to  $^5F_5$  will likely occur, at least at higher concentrations, and these may actually enhance population levels in  $^5I_5$ , thereby improving prospects for producing inversion on the  $^5I_5 \Rightarrow ^5I_6$  transition at 3.9  $\mu\text{m}$ . More detailed experimentation is, however, required to explore the relative contributions of the  $^5S_2$  and/or  $^5F_5$  levels in the two Ho-doped materials.

Excitation spectra were also taken in order to gather further information as to the strength of the 750 nm absorption processes. For example, Figure 4.9 shows the excitation spectrum for 752 nm emission in 1% Ho:BYF. The spectrum shows the expected peaks at 540 nm and 450 nm but no peak at 660, indicating that at this low concentration, the 752 nm transition between the ground state and  $^5I_4$  (to which  $^5F_5$  relaxes) is much weaker than the 750 nm transitions to higher levels. This is in agreement with the 750 nm absorption measurements shown in Figure 4.2 (see previous subsection). The excitation data do not give evidence which of the levels -  $^5G_6$  or  $^5S_2$  - play the more important role in producing 750 nm transitions. The situation does not appear to change much for higher concentration material. For example, the excitation spectrum shown in Figure 4.10 for a 20% Ho:YLF sample at the same emission wavelength, also does not reveal any peaks near 660 nm. We therefore conclude that there is strong 750 nm emission from (or absorption to) levels above  $^5F_5$ , which can be  $^5S_2$  or higher, in both Ho:YLF and Ho:BYF.

#### 4.1.3 Lifetime Measurements

For the lifetime measurements, the second harmonic of a pulsed Nd:YAG laser was used with a pulse duration of 20 ns. The radiation is focused into the sample and the fluorescence detected with a 0.3m monochromator. A band pass filter provides additional suppression of scattered light. A PMT is used for detection of the fluorescence decay. Time dependent fluorescence data were acquired with a 2 Gbit/s, 400 MHz scope. These were plotted and lifetimes calculated using the standard 1/e method.

Excitation Spectrum of BYF:Ho 1% at Emission  
Wavelength 752nm

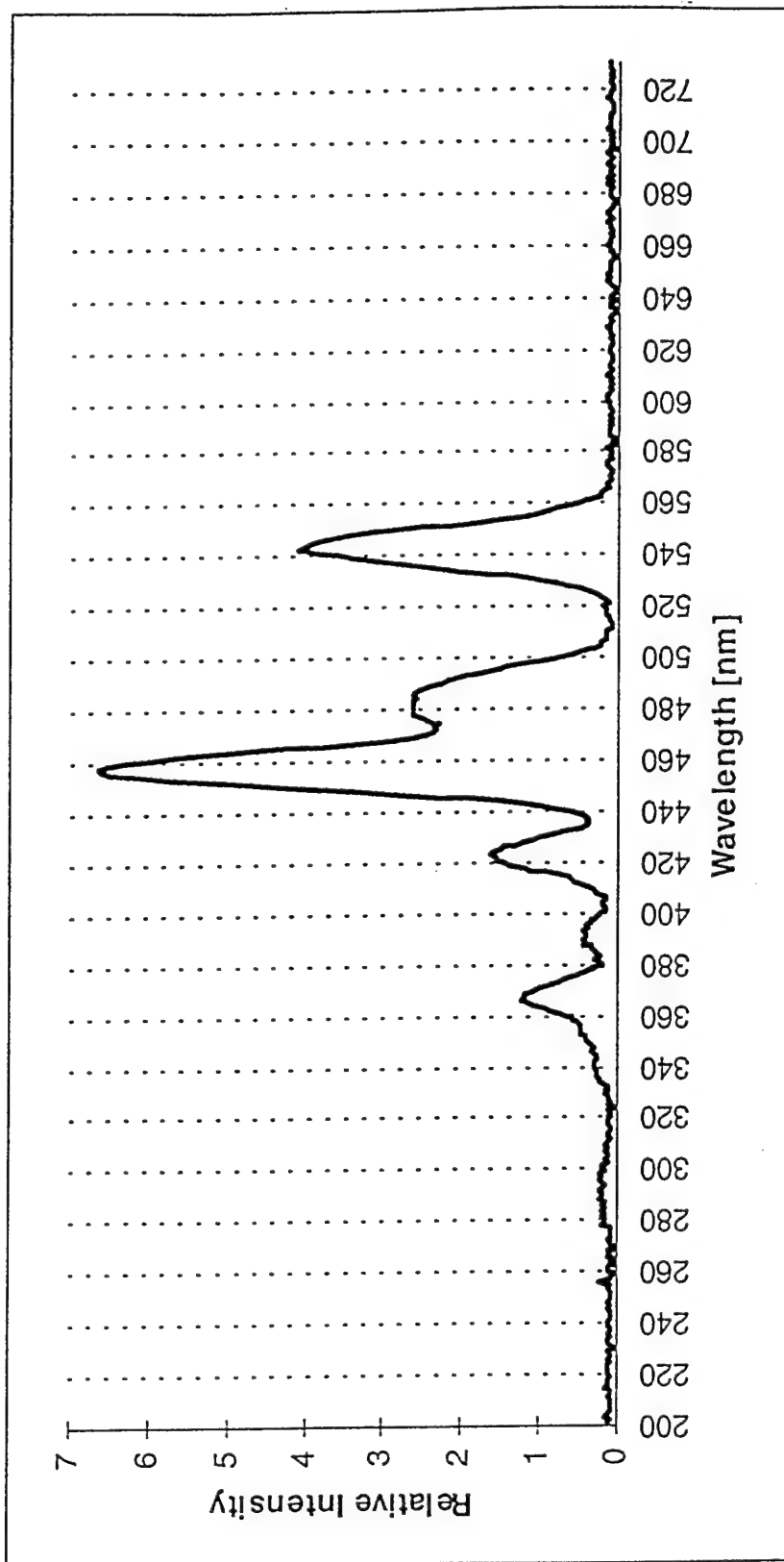


Figure 4.9

Excitation Spectrum of YLF:Ho 20% at Emission  
Wavelength 753nm (random polarization)

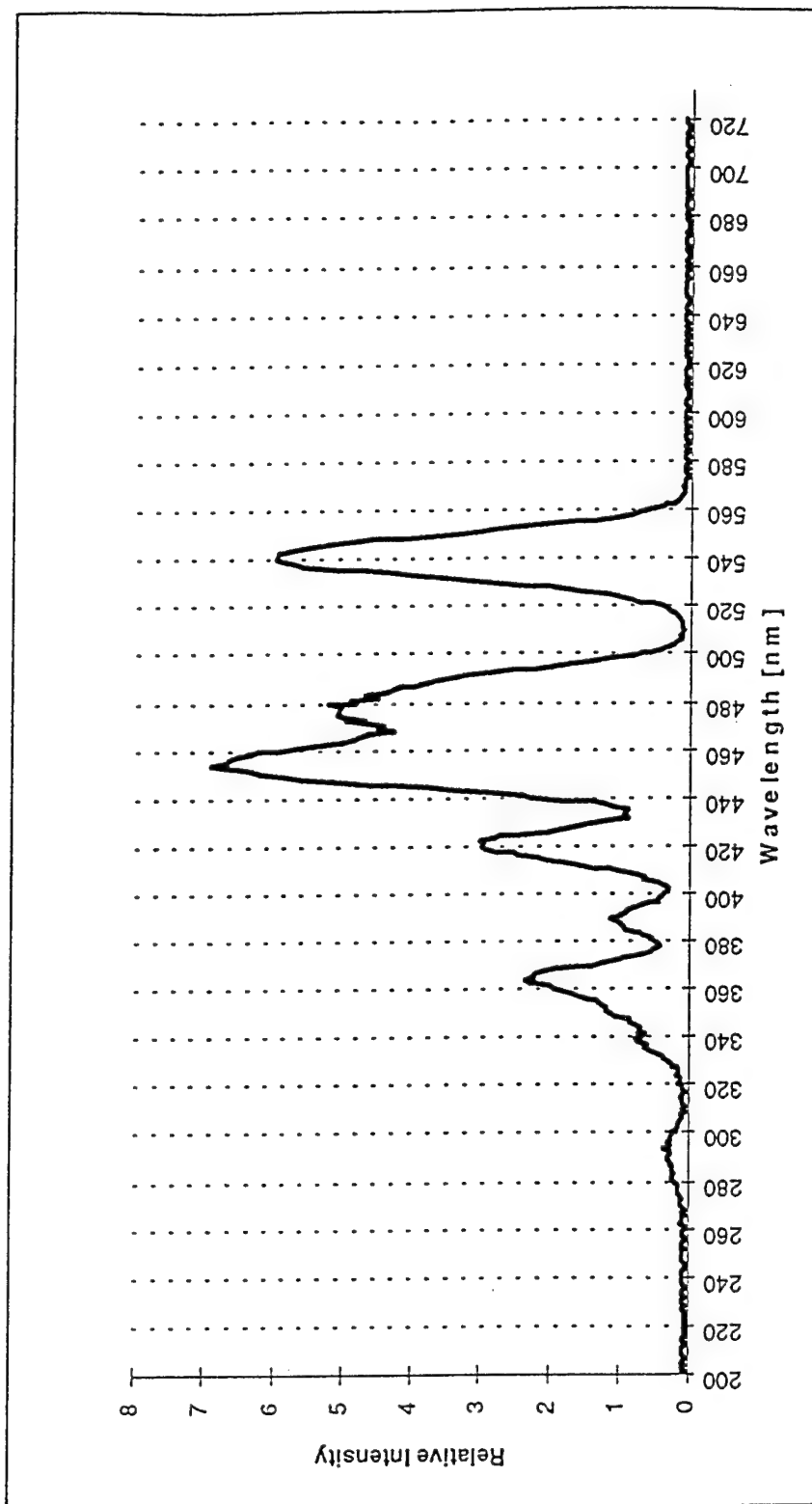


Figure 4.10

The radiation at 532 nm excites ions into the  $^5S_2$  level as evidenced by the fact that the time dependent emissions measured at 540 and 752 nm (both from  $^5S_2$ ) were the same. Lifetime measurements were carried out on all seven samples: 1%, 10% and 20% Ho:BYF and 1%, 2%, 10% and 20% Ho:YLF. Examples of the data taken and resultant lifetime calculations are shown in Figures 4.11 and 4.12 for Ho:YLF in low concentration and high concentration materials, respectively. Similar data are available for Ho:BYF. Results for fluorescence decay lifetimes from the  $^5S_2$  level can be summarized as a function of concentration as follows:

Ho:YLF	concentration	1%	2%	10%	20%
	lifetime ( $\mu$ s)	97	70	5.2	2
Ho:BYF	concentration	1%		10%	20%
	lifetime ( $\mu$ s)	284.5		15.5	3.7

The apparently strong decrease in  $^5S_2$  lifetime as a function of increasing concentration reflects a respective increase in cross relaxation rates, as predicted.

## 4.2 Z-scan Fluorescence Experiments

Studies of pump absorption and Z-scan fluorescence emissions provide a direct indication of population build-up at specific levels. The efficiency of fluorescence is measured as a function of the axial position of a lens which focuses the pump laser i.e., pump intensity. The lens is generally mounted on a micrometer translation stage to permit translation of the focus with respect to the sample, resulting in an accurate measurement of the relative pump intensity as a function of lens position.

The pump laser source set up for these initial measurements consisted of a cw Ti:sapphire laser pumped by an 8W Ar+ laser. The laser could provide up to 1 W of radiation continuously tunable from 710 nm to 760 nm. The output of the Ti:sapphire laser is directed through a polarization rotator to allow for optimal alignment of the linearly polarized Ti:sapphire beam with the c-axis of the Ho-doped crystals. A beam splitter directs a portion of the beam to a wavemeter to monitor the pump wavelength.

The fluorescence was measured at the following wavelengths: 540, 900, 1200 and 2060 nm, representing emissions from the  $^5S_2$ ,  $^5I_5$ ,  $^5I_6$  and  $^5I_7$  levels, respectively to the  $^5I_8$  ground state. These emissions are important

# Lifetime measurements for 5S2 level for 1% and 2% Ho:YLF

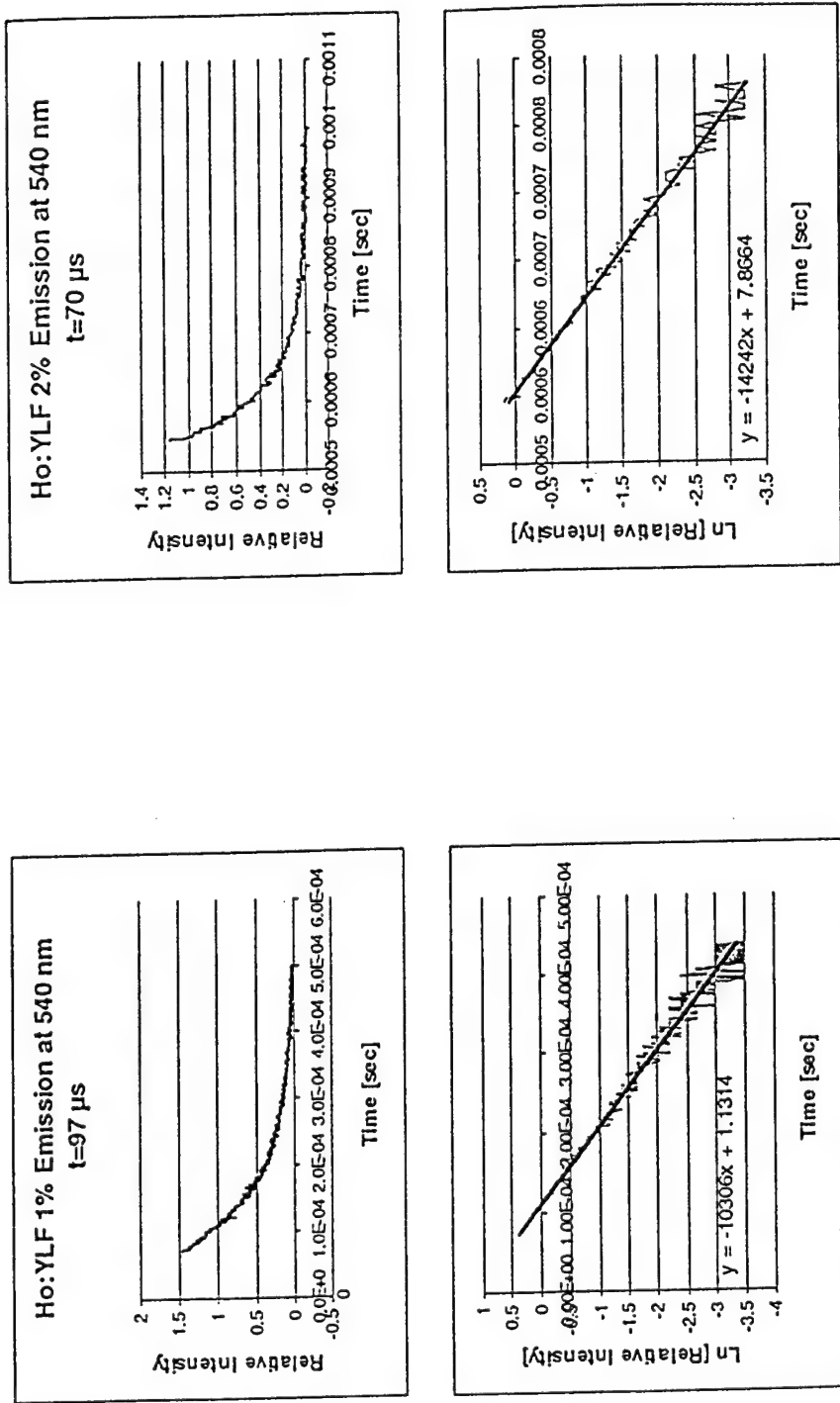


Figure 4.11

# Lifetime measurements for 5S2 level for 10% and 20% Ho:YLF

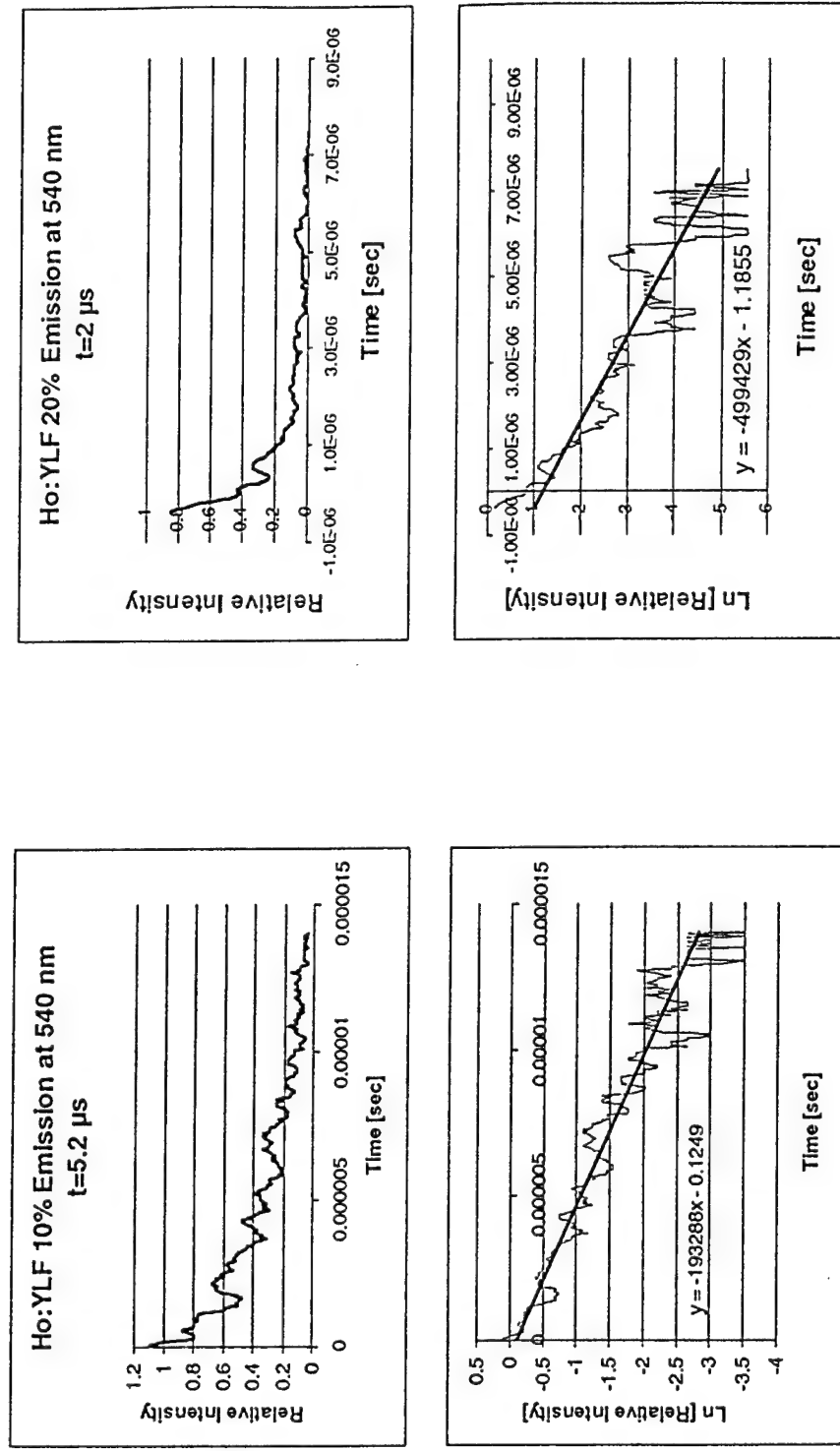


Figure 4.12

as they provide a direct indication of population build-up at the various levels upon pumping with near-IR photons. An increase in the green emission at 540 nm as a function of increasing pump intensity is taken as evidence of two-photon absorption to the  $^5S_2$  level, while a corresponding increase in the 900 nm emission is indicative of both two-photon excitation and cross relaxation process from the  $^5S_2$  level to  $^5I_4$ , followed by rapid relaxation to the  $^5I_5$  level, which is the upper level of the desired 4  $\mu\text{m}$  transition.

Different detectors were used to best detect emissions at the various wavelengths. Thus, a silicon photodiode with appropriate band-pass filters is used to detect the 540 nm and the 900 nm emissions. A germanium detector is used to detect radiation at 1200 nm. The same detector could also be used to monitor the radiation at 900 nm again, which provided a double check against measurements performed with the silicon detector. An InSb detector, also with an appropriate band pass filter is used to detect radiation at 2060 nm. Since this detector could also be used to detect the 1200 nm emission, using a different filter, this again provided a second check on the preceding measurements conducted with the germanium detector.

Generally, Z-scan measurements with 10% and 20% Ho:YLF and Ho:BYF samples show substantial increase in green emission at 540 nm as the intensity increases, with the expected quadratic dependence on pump power, indicative of two photon absorption at 750 nm. In lower doped samples (1%  $\text{Ho}^{3+}$ ) the emission at 900 nm is rather weak. In the prior SBIR project this emission showed a marked (and nonlinear) increase as a function of pump intensity at higher concentrations in Ho:YLF, which was taken as an indication of significant contributions from cross relaxation processes. Similar results were seen in the case of Ho:YLF, with the trend of sharp increases in the 900 nm emission at higher concentration continuing out to 20% Ho, as shown in Figure 4.13.

Significant differences emerge however between Ho:YLF and Ho:BYF. In the case of 900 nm emission the differences are highlighted in Figure 4.14, which shows that there is no increase in the emission for Ho:BYF between the 10% and 20% samples, and there may even be a decrease, in sharp contrast to the situation for Ho:YLF. The intensity of emission is, however, higher for both the 10% and 20% Ho:BYF samples than the 10% Ho:YLF samples by about a factor of 2, showing higher effective cross relaxation rates for the former. Cross relaxation is strongest, however, for the 20% Ho:YLF. These differences should, however, be considered qualitative as the

## Emission at 900 nm with germanium detector and bandpass filter

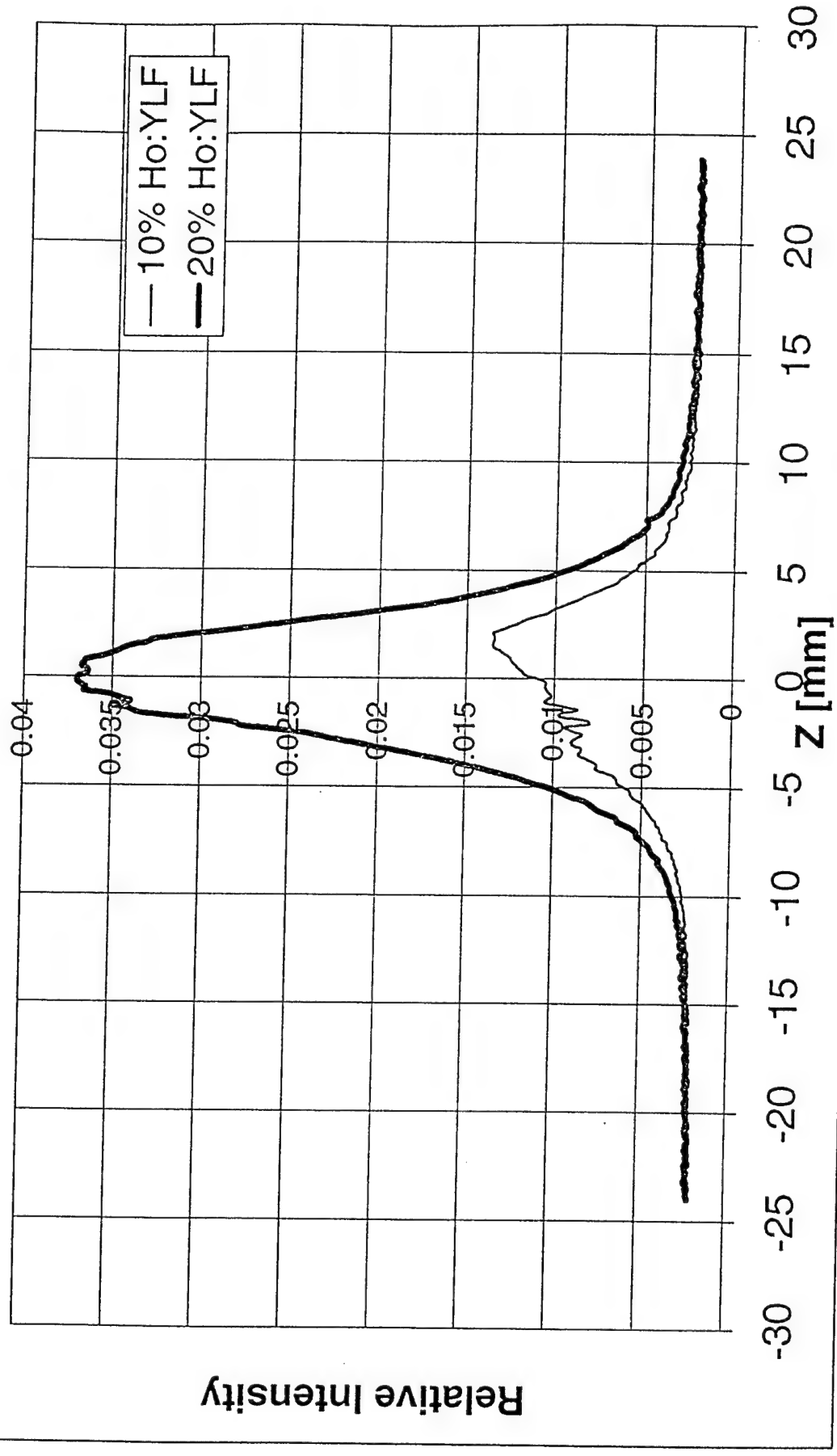


Figure 4.13

### Emission at 900 nm with germanium detector and bandpass filter

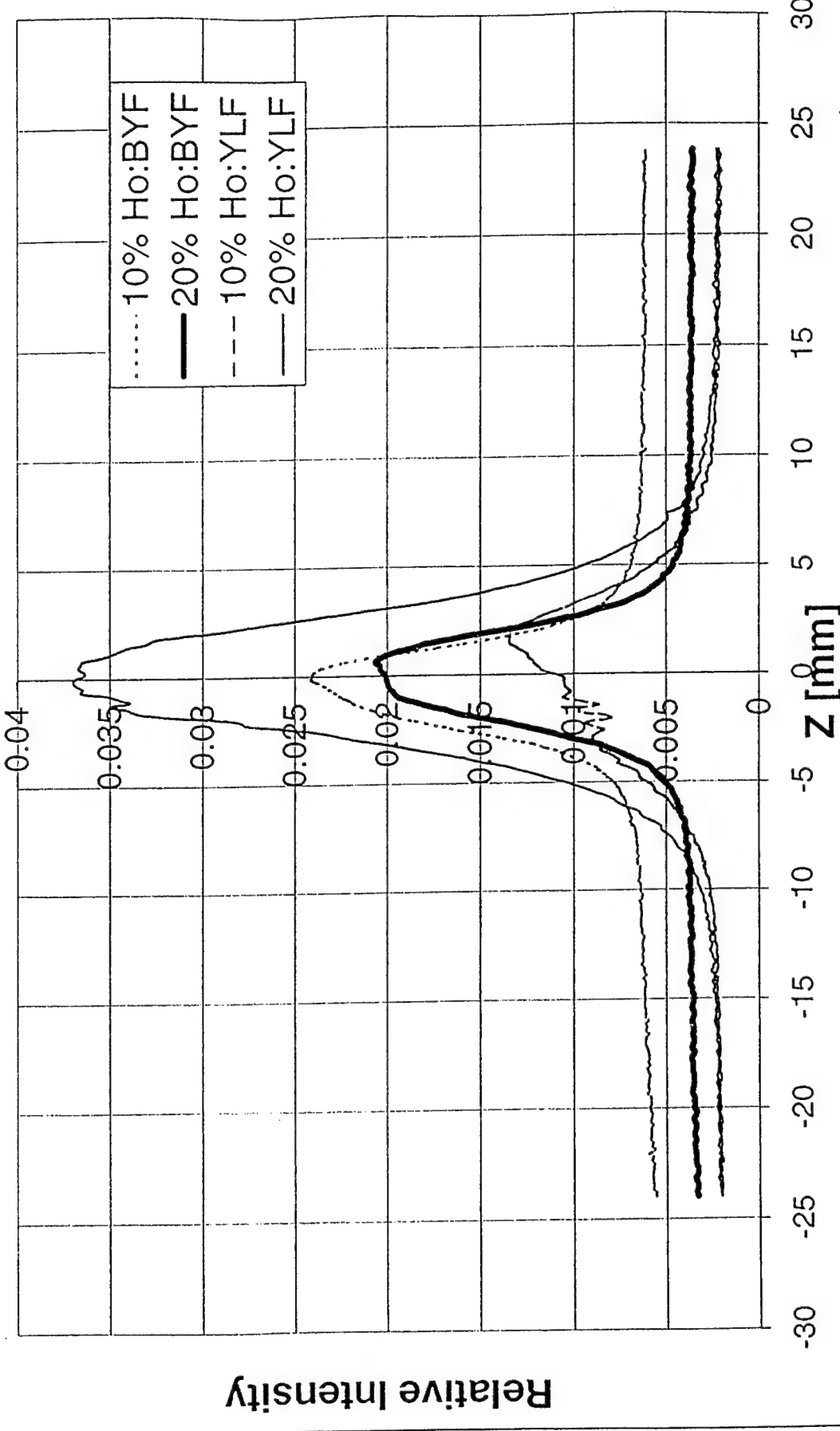


Figure 4.14

conditions under which different Z-scan measurements were taken were not always identical.

Even more curious is the behaviour of the 1200 nm emission line in Ho:BYF. Figure 4.15 shows a strong drop in the emission intensity at higher pump intensities in 10% Ho:BYF, as measured with an InSb detector. The same effect is observed with the germanium detector as well, as shown in Figure 4.16. This figure also shows the relative fluorescence efficiencies from  $^5I_6$  at 1200 nm as compared to the previously measured emission intensity from  $^5I_5$  at 900 nm, both in 10% Ho:BYF. The drop in 1200 nm emission is seen as much sharper than the relatively small increase of the 900 nm emission. This effect persists to higher Ho concentrations as shown in Figure 4.17, where the behavior for the 10% and 20% samples are compared. It is also notable that Ho:YLF does not display the decrease in 1200 nm emission seen in Ho:BYF as also shown in Figure 4.17. It is not clear at this time what process causes the drop in  $^5I_6$  emission in Ho:BYF. This could be due to an upconversion process from  $^5I_6$  to some higher lying level. It could, however, also be due to an increase in the absorption of the 750 nm radiation from the  $^5I_6$  level at higher pump intensities.

To test the latter hypothesis, the 490 nm emission was measured for both the 10% and 20% Ho:BYF samples as shown in Figure 4.18. The increase in emission at higher intensities indicates that some mechanism is in place elevating photons to the upper  $^5G_6$  level. This mechanism could be due to another absorption of pump photons at 750 nm (three-photon absorption), but may also be due to any one of several upconversion processes. In Ho:BYF, the effect is not strongly concentration dependent. It is however stronger than in Ho:YLF, as shown in Figure 4.19 where 20% samples of Ho:BYF and Ho:YLF are compared.

Thus there appears to be some mechanism at work that helps empty the long lived  $^5I_6$  level, which may or may not be related to an additional absorption of pump photons from that level. We consider these newly observed features to be encouraging, since they provide, for the first time an indication that there may be a way of breaking the bottleneck at the  $^5I_6$  level, at least in Ho:BYF. At the same time, however, we note that cross relaxation from  $^5S_2$  to  $^5I_5$  as a way of building up population in the latter does not appear to be as effective in Ho:BYF at higher concentrations as it was in Ho:YLF. Since Ho:YLF also does not display the decrease in 1200 nm emission seen in Ho:BYF (see Figure 4.17), it may be that the two features (the concentration independent increase in emission from  $^5I_5$  and a reverse concentration dependent decrease in  $^5I_6$  emission) are related, but it is not yet clear how.

Emission of 10 % Ho:BYF at 1200 nm with  
InSb detector and bandpass filter

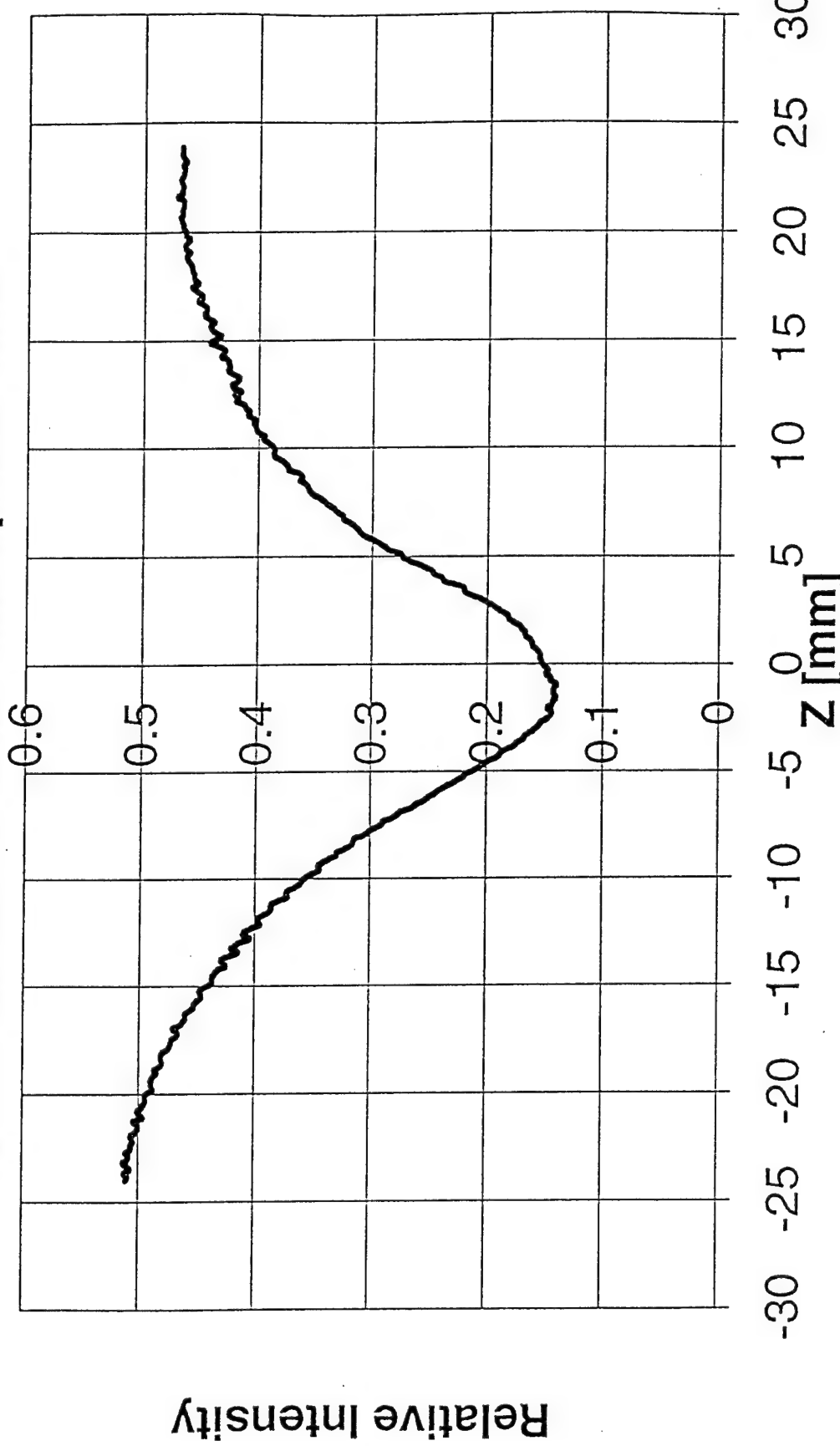
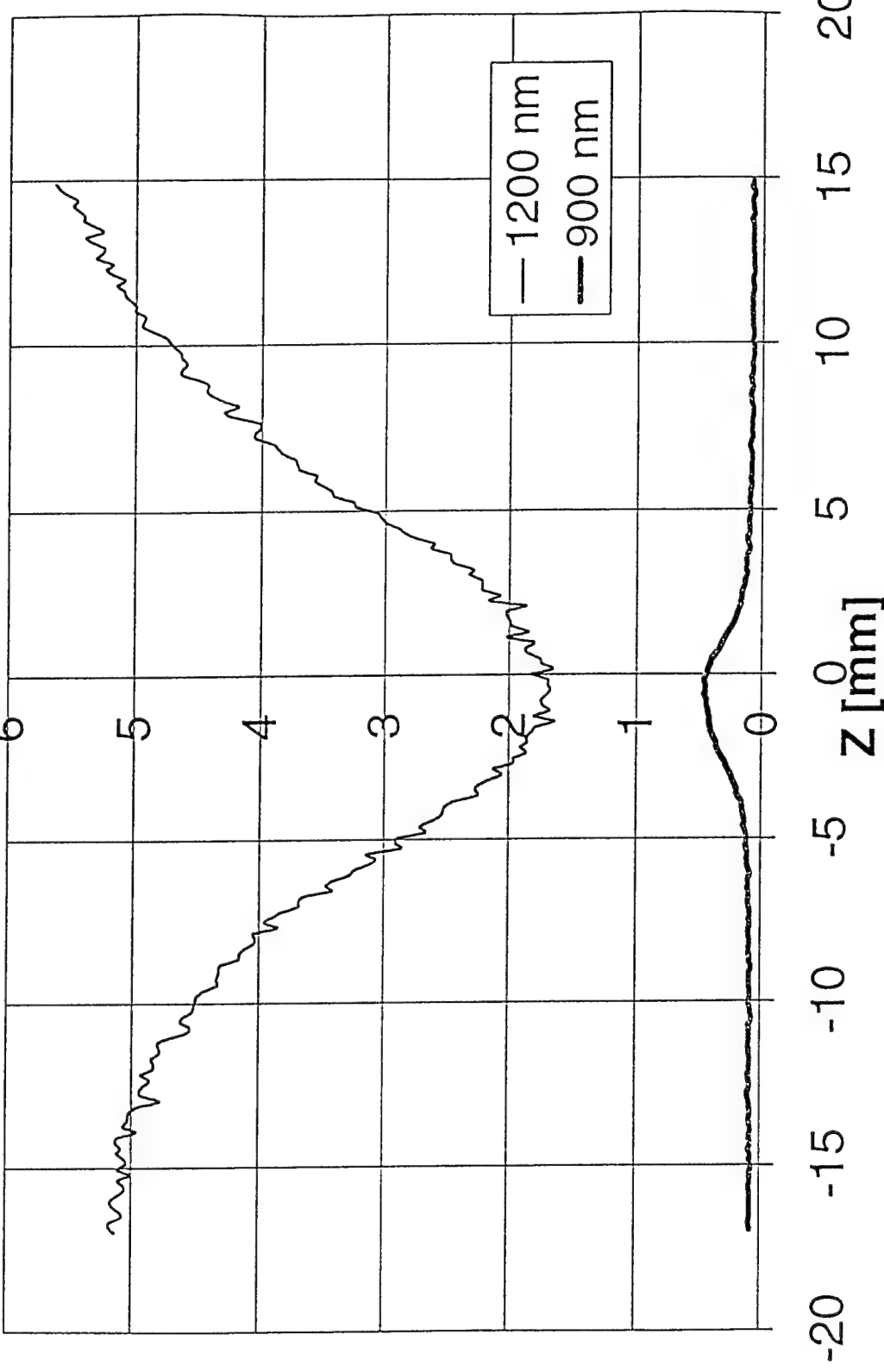


Figure 4.15

Emission of 10 % Ho:BYF at 1200 nm and 900 nm with  
germanium detector and bandpass filters



Relative Intensity

Figure 4.16

Emission at 1200 nm with germanium detector and bandpass filter

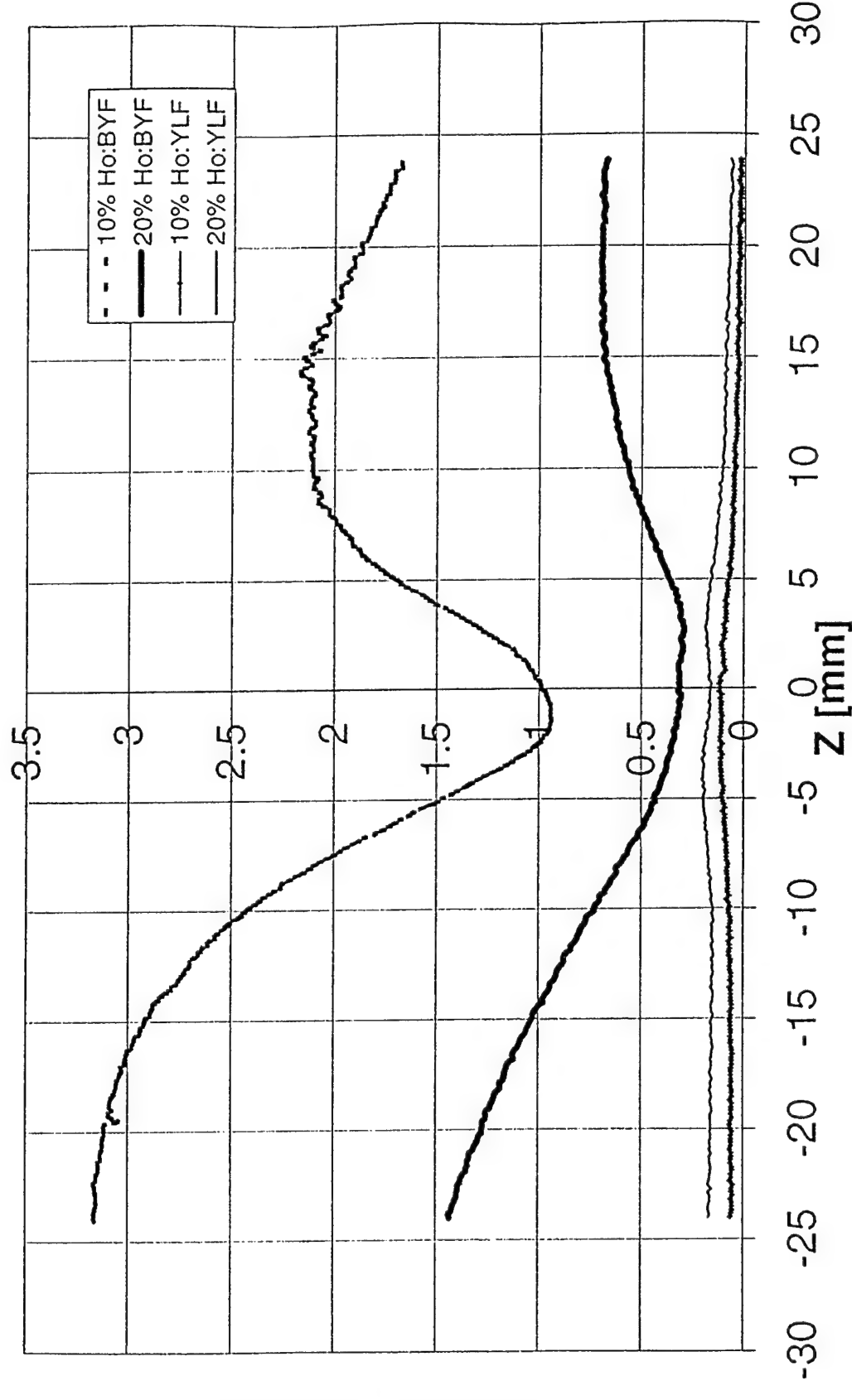


Figure 4.17

Emission at 490 nm with silicon detector and bandpass filter

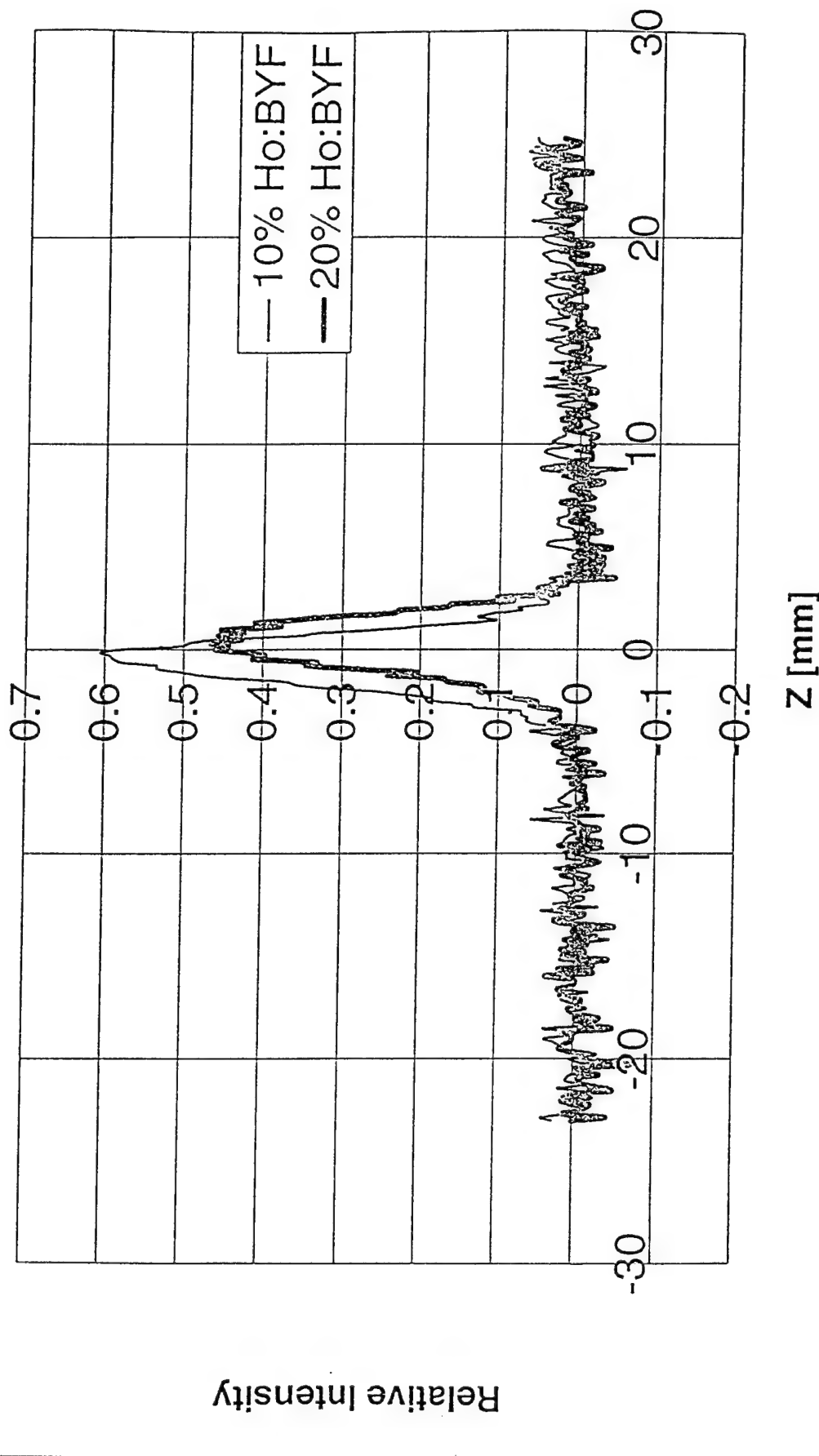


Figure 4.18

Emission at 490 nm with silicon detector and bandpass filter

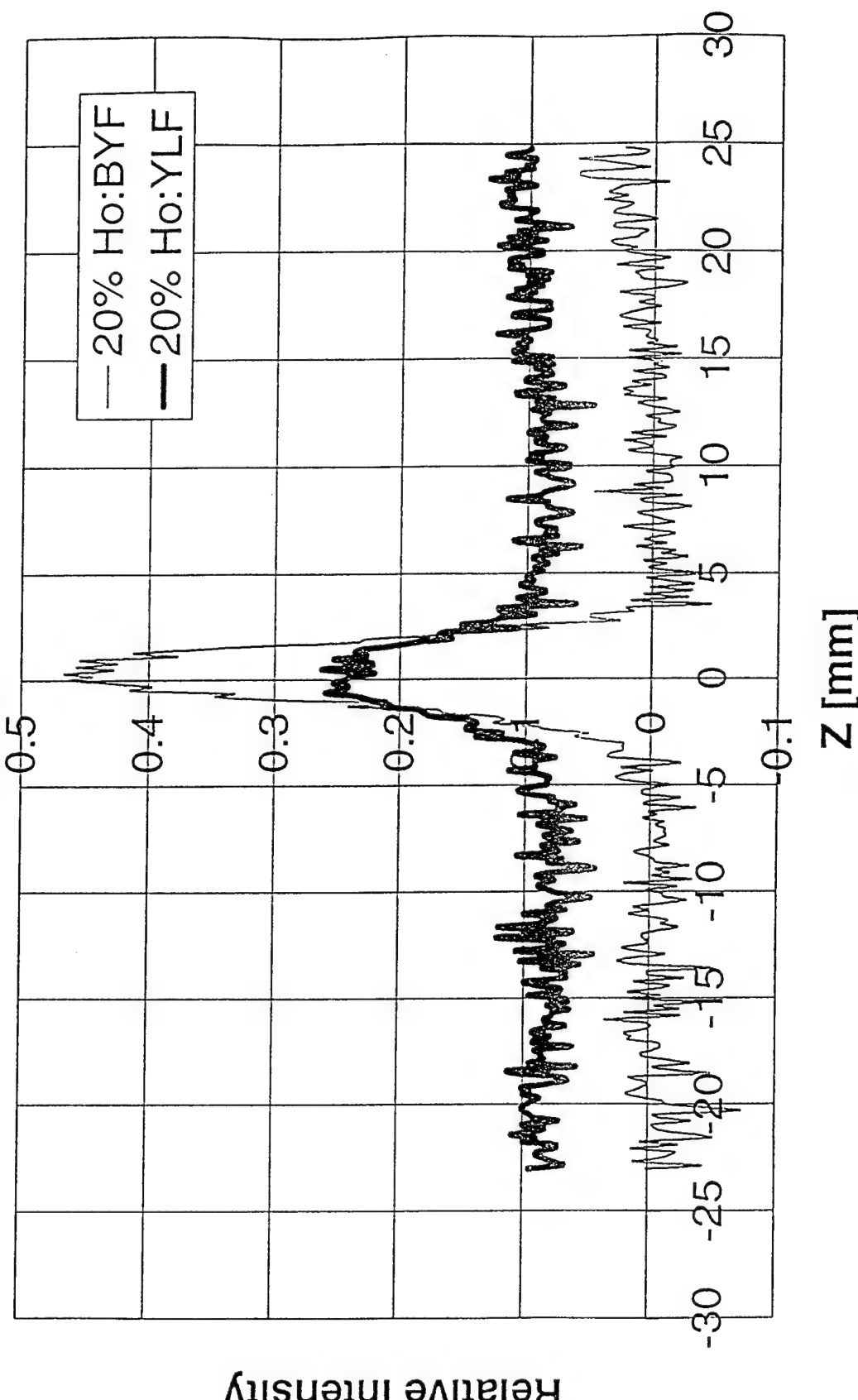


Figure 4.19

There were also some interesting features displayed in the 2060 nm emission data, reflecting population build-up in the very long lived  $^5I_7$  level. Figure 4.20 shows a comparison between emissions at 1200 and 2060 nm for 10% Ho:BYF. Thus, while the  $^5I_6$  emission drops continuously as the pump intensity increases, the 2060 nm fluorescence first increases with increasing pump intensity but then drops at the highest intensity. This is, to some extent, expected from the model. Thus, due to the long lifetime of the  $^5I_7$  level, its population will first build up, but as pump intensity increases, more ions will be elevated to  $^5S_2$  by accelerated absorption of 750 nm photons, leading to depletion of the level at very high intensities.

The depletion of  $^5I_7$  at high intensity is also observed in Ho:YLF. Figure 4.21 compares the behavior of the 2060 nm emission in 10% and 20% samples of both Ho:BYF and Ho:YLF. A similar depletion trend is seen in the two materials, probably reflecting the similarity in  $^5I_7$  lifetimes (14-16 ms). The reasons for the observed asymmetry of the emission curves for Ho:BYF as compared with Ho:YLF, are not yet clear.

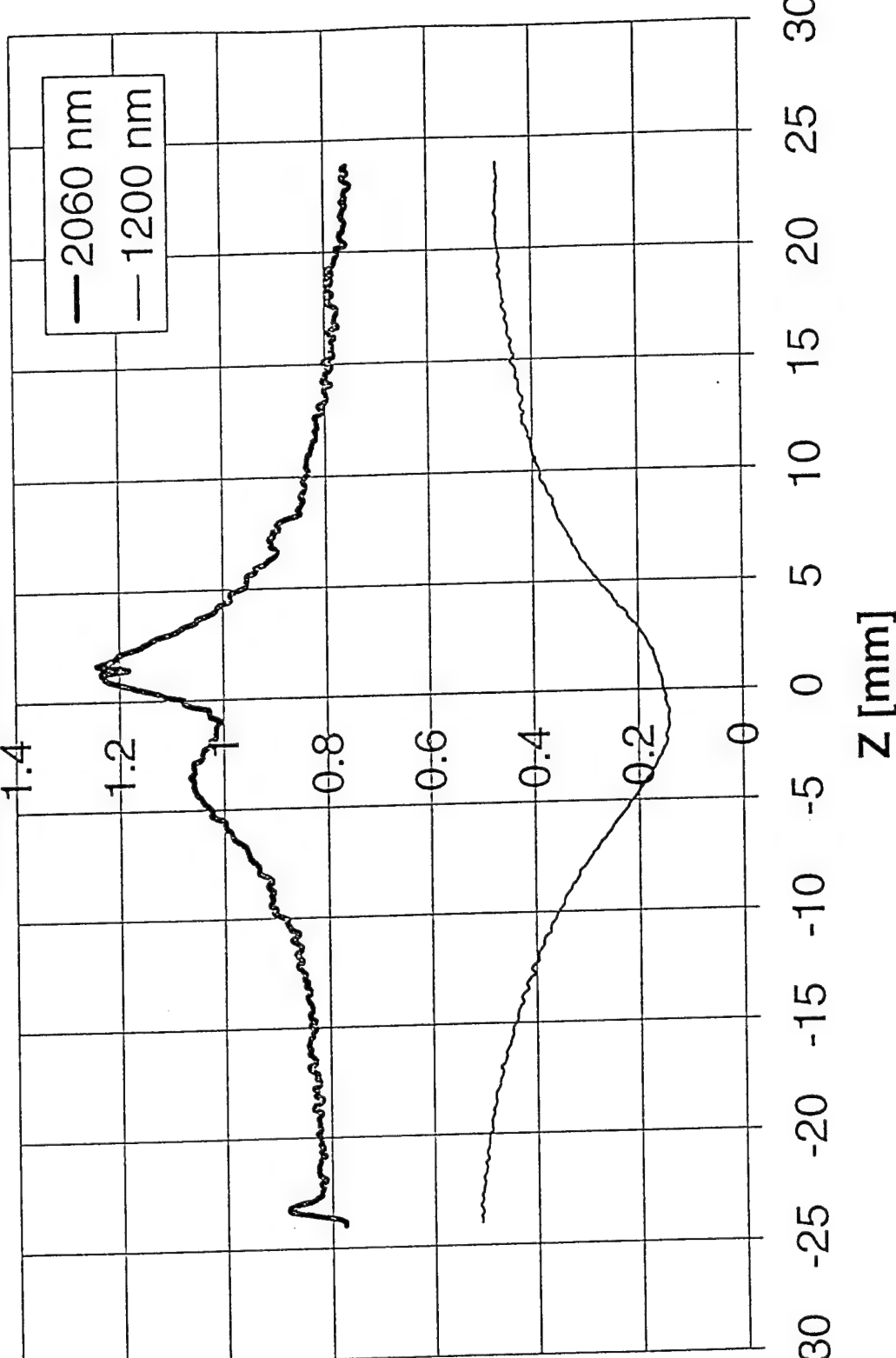
Finally, Figure 4.22 shows results from measurement of 640 nm fluorescence for both 10% and 20% samples of Ho:YLF and Ho:BYF. The emission is similar for the two 10% samples but rises dramatically for the 20% Ho:BYF. This can be attributed to a strong contribution from a  $^5F_3 \leftrightarrow ^5F_5$  cross relaxation process in Ho:BYF, but not in Ho:YLF. The validity of such a hypothesis is dependent on the existence of sufficiently strong absorption at 750 nm to the upper  $^5G_6$  level in the former.

One caveat that applies to all the Z-scan experiments is that results may be somewhat modified if the rise in temperature of the sample as the intensity increases is taken into account. This may result in a scale factor affecting the magnitude of the relative intensity curves near the center. Also, we believe that a series of experiments should be carried out under more controlled conditions, so that more quantitative comparisons between different samples could be carried out.

Thus, a number of additional spectroscopic and Z-scan measurements should be carried out to more conclusively identify the excitation and cross relaxation mechanism involved in higher concentration Ho-doped fluoride crystals. For example, Z-scan absorption measurements at 750 nm for Ho:BYF at different concentrations would be useful, especially when compared to Ho:YLF. Thus, on the previous SBIR project, a dramatic increase in the intensity of absorption was seen in 10% Ho:YLF, which was interpreted as evidence of strong absorption from the  $^5I_7$  level of the 750 nm pump radiation - with a cross section on the order of  $4 \times 10^{-20} \text{ cm}^2$ . In Ho:BYF, the

Emission of 10 % Ho:BYF at 1200 nm and 2060 nm with

InSb detector



Relative Intensity

Figure 4.20

### Emission at 2060 nm with InSb detector and bandpass filter

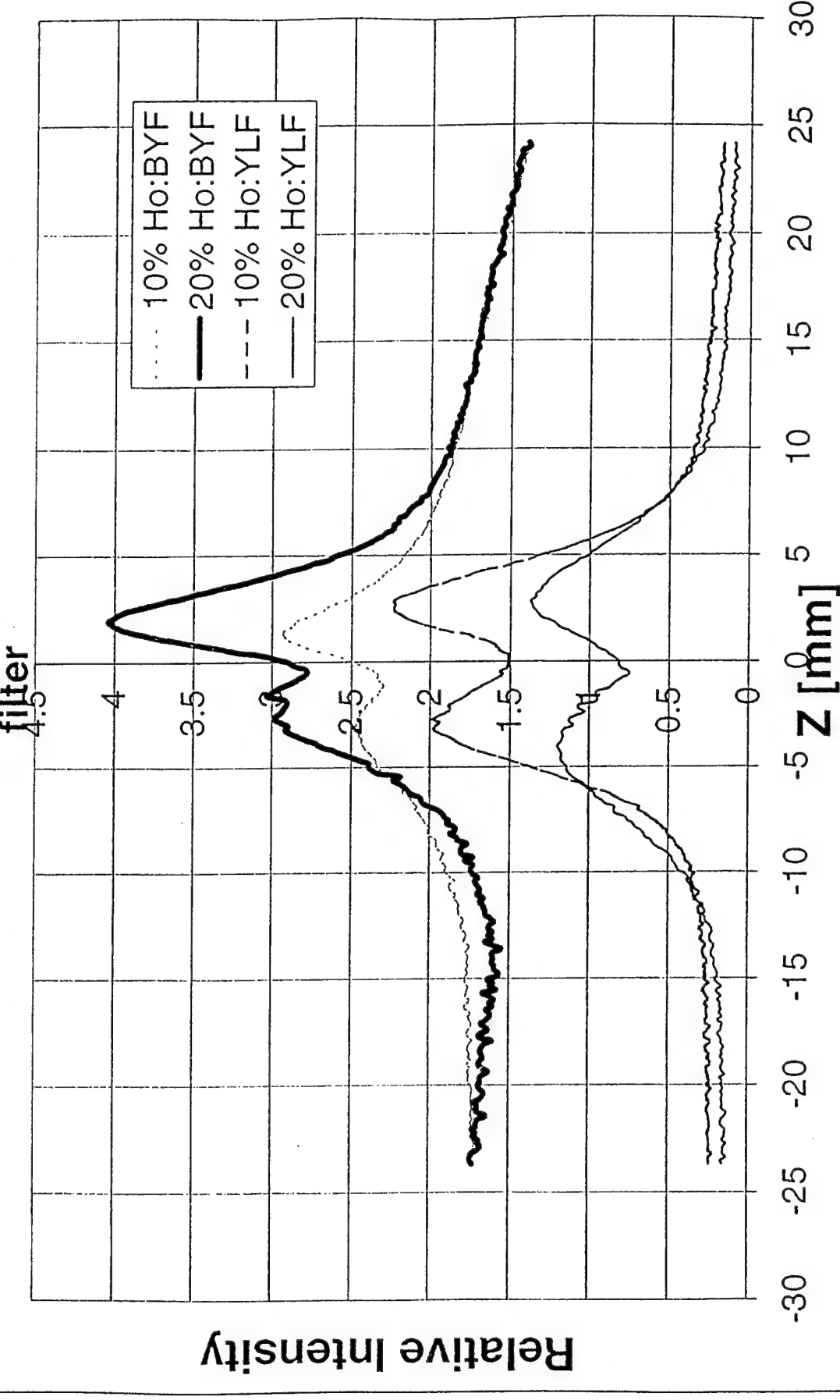


Figure 4.21

## Emission at 640 nm with silicon detector and bandpass filter

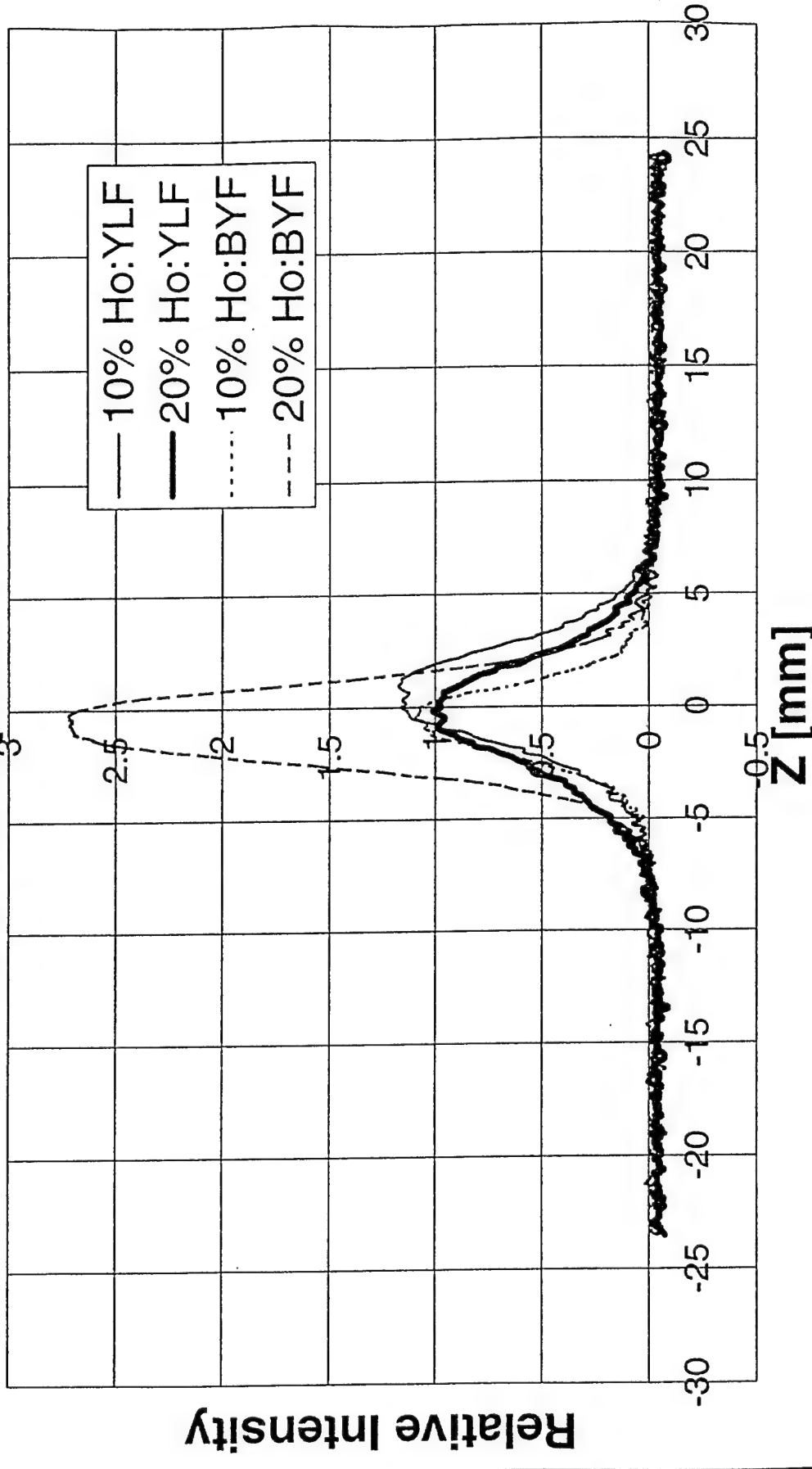


Figure 4.22

possibility of three-photon absorption was not ruled out and careful intensity-dependent absorption measurements may help confirm or deny this conjecture.

In addition, in Ho:BYF there may be important contributions from upconversion processes, which may modify the rates of cross relaxation processes. Thus, the postulate of 750 nm absorption to  $^5S_2$  followed by cross relaxation to  $^5I_4$  may be too simple for Ho:BYF. Both emission and excitation spectra indicate that an alternative (or additional) cross relaxation process involving the  $^5F_5$  level may be operable in this material following excitation to the high lying  $^5G_6$  multiplet. In particular, there may various alternative excitation and emission paths involving upconversion processes, some of which can be tested through additional spectroscopic measurements extending to more wavelengths in the IR. We believe that such measurements may yield considerable dividends given the promising early indications that it may be possible to break the bottleneck at  $^5I_6$  as well as (or in addition to) the one in the  $^5I_7$  level, thus raising hope of efficient laser action at 3.9  $\mu\text{m}$  and/or 2.9  $\mu\text{m}$ .

#### 4.3 Short Pulse Laser Experiments

To validate feasibility of producing the 3.9  $\mu\text{m}$  radiation from the  $^5I_5 \Rightarrow ^5I_6$  transition in a cascade with a  $^5S_2$  to  $^5I_6$  transition at 1.4  $\mu\text{m}$ , lasing experiments using direct resonant pumping with a short pulse green laser were carried out on this program. This is similar to what was originally done by Esterowitz et al<sup>1</sup>, but using an end-pumping arrangement. In our experiments, the green beam comprises radiation from a frequency doubled, Q-switched 10 ns Nd:YAG laser, available at CREOL. The laser operates at 5-10 Hz, which is sufficiently low to avoid the self-termination problems due to the long lived  $^5I_6$  and  $^5I_7$  states. It was hoped that results from the direct lasing experiments could also provide additional useful data for the Ho laser system, including estimates of stimulated emission cross sections and level lifetimes, which could be checked against parameters calculated independently from spectroscopic measurements. It was also hoped that lasing tests with pumping at 532 nm will help set damage limits and also establish requirements for tolerable levels of losses in a possible fiber laser.

Green beam pumped laser experiments conducted on the previous SBIR project were not successful due to optics damage issues compounded by insufficient pump energy. As part of this project, laser tests were conducted at CREOL, using a laser with a higher output energy. Originally, experiments were conducted on existing rods fabricated from 2% Ho:YLF. The

rods were about 2 mm in diameter and 1.5 cm long. It was not AR-coated since it was determined that losses would not be much lower than Fresnel losses. Dichroically-coated cavity optics previously acquired from RMI were made available to this project. The optics consisted of two short (10 cm) focal length mirrors coated for maximum reflection at 3.9  $\mu\text{m}$  and 1.4  $\mu\text{m}$  (>99%) and maximum transmission for wavelengths in either the green or near-IR, assuming a longitudinal pumping arrangement. Actual measured green beam transmission was around 85%. With these two mirrors a short (18-20 cm) nearly spherical cavity was formed, allowing maximum pump beam diameter on the input mirror (to minimize damage) but minimum diameter in the rod (to maximize intensity). The first experiments were not successful, which was attributed to poor absorption of the 532 nm radiation by the low concentration rods. The experiments were then repeated using laser samples of 10% Ho:YLF.

While the 532 nm wavelength is still not coincident with the peak of the absorption for Ho:YLF, (where it was determined to be centered at around 535-536 nm), it was hoped that this time, with the higher Ho concentration rod, the absorption would be adequate given sufficient absorption length. We were encouraged by the fact that a short pulse pump of this wavelength was successfully utilized in the early experiments conducted by Knights, et al<sup>3</sup> (which demonstrated linear downconversion to 750 nm) with over 90% absorption in a Ho:YLF material of low concentration but 5 cm length. By contrast, the arrangements used in Refs. 1 and 2 utilized transverse pumping which provided much shorter (less than 0.5 cm) absorption depths and necessitated utilization of a green wavelength closer to the absorption peak. We performed measurements of 532 nm absorption which confirmed that absorption in the 10% sample is considerably higher than in the 2% Ho:YLF rod used previously. Specifically, for the 10% Ho:YLF the measured absorption coefficient (in the  $\pi$  polarization) at 532 nm is 2.8  $\text{cm}^{-1}$ , increasing to 5.6  $\text{cm}^{-1}$  for 20% Ho:YLF. (The absorption expected in Ho:BYF is somewhat lower - only 2  $\text{cm}^{-1}$  in a 10% Ho concentration). In either case these are much higher than the 0.6  $\text{cm}^{-1}$  absorption measured for the 1% samples. Thus, for the 10% Ho:YLF sample, we estimated that threshold for 1.4  $\mu\text{m}$  lasing would be achieved with a pump energy of less than 50 mJ. This energy was available from the laser but the main issue was damage to the mirrors, since damage thresholds for IR coatings for pulsed beams are notoriously low, less than 4-5 J/cm<sup>2</sup>, at best.

After some effort, lasing was achieved for pumping at both 750 nm and 532 nm. A trace of the laser pulse at 1.4  $\mu\text{m}$  is shown in Figure 4.23. Threshold for the 1.4  $\mu\text{m}$  laser was quite low - less than one mJ. Unfortunately, problems encountered with the pump laser prevented full

10% Ho:YLF 1.4 micron laser pulse

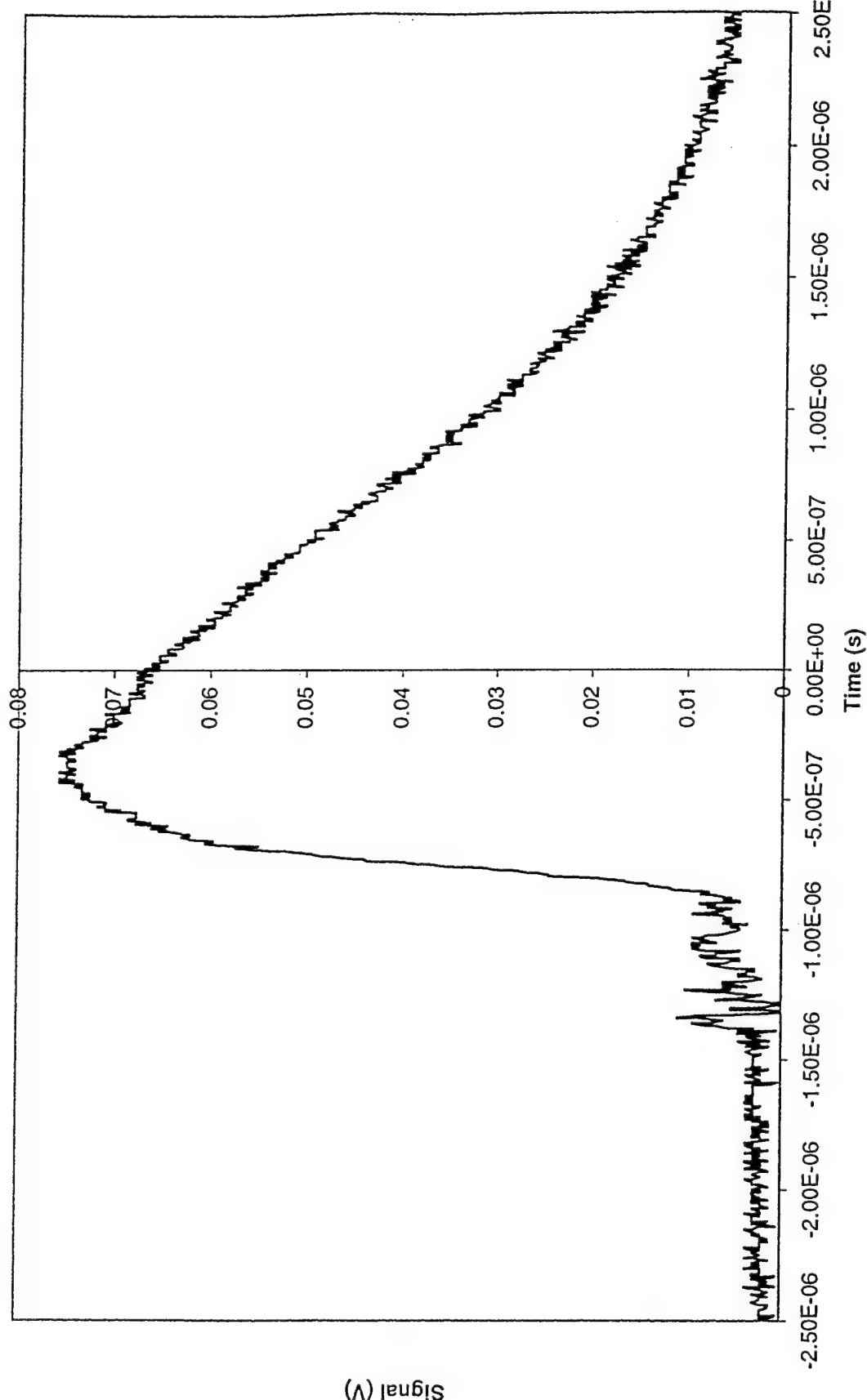


Figure 4.23

characterization of the laser action. We were also not able to test for laser action at 4  $\mu\text{m}$  because of a lack of a sensitive enough detector for that wavelength. A mirror with more optimal outcoupling would also be likely necessary for 4  $\mu\text{m}$  lasing, but this exceeded the resources available to the phase I program. We nonetheless take encouragement from the fact that lasing action was achieved at 1.4  $\mu\text{m}$  with a very low threshold. Potentially this could be an efficient laser on its own merits. Indeed, this line was successfully lased in the past, using flashlamp pumping at room temperature<sup>5</sup>.

## V. Conclusions

Again, the objective of this project was to establish the feasibility of producing radiation at multiple wavelengths in the infrared from a single solid state laser medium. Significant progress was made toward this objective during this project. A brief summary of that progress is:

- Laser quality boules of high concentration Ho:BYF have been grown and evaluated;
- Major improvements in the laser modeling of the Ho system were made by including cross relaxation terms and resonant pumping of several levels;
- The model results show that by reducing the  $^5I_6$  level population an inversion of the 3.9  $\mu\text{m}$  line will result;
- Using absorption spectroscopy the cross sections of several important transitions were measured for different Ho concentrations;
- The fluorescent lifetimes were measured for several important transitions as a function of Ho concentration;
- The absorption and fluorescent data provided important results on the cross-relaxation of several levels of the Ho system as a function of concentration that were input into the model;
- Z-scan fluorescence measurements were made which provided important information on the population buildup of several levels as a function of concentration and pump intensity;
- In laser tests, lasing was observed at 1.4  $\mu\text{m}$  and 750 nm in 10% Ho:YLF. An extremely low threshold of less than one millijoule was observed for the 1.4  $\mu\text{m}$  line;
- Single crystal fibers of Ho:YLF and Ho:BYF were grown but laser quality has not yet been achieved. Important improvements in quality were obtained by reducing the oxygen concentration in the melt zone and by flux-doping of the melt.

From our list of achievements it can be seen that much progress was made and all indications are that the final objective of a multiwavelength

efficient solid state laser system can indeed be achieved. As such a system would have many military and commercial applications, continued development is certainly justified.

## REFERENCES

1. L. Esterowitz, R. C. Eckardt, and R. E. Allen, *Appl. Phys. Lett.*, **35**, 236 (1979); see also  
R. C. Eckardt, L. Esterowitz, and Y. P. Lee, *Proc. Int'l Conf. Lasers*, 1981, p. 380 (1981)
2. G. Y. Gilliland et al, OSA proceedings of Advanced Solid State lasers conference, WE4-1, p. 211 (1987) - Ho:BYF lasing at 2.9  $\mu\text{m}$
3. Johnson & Guggenheim, *IEEE J. Quantum Electron.*, **QE-10**, 442 (1974)
4. M. G. Knights, W. F. Wing, J. W. Baer, E.P.Chicklis and H. P. Jenssen, *J. Quantum electron.* **QE-18**, 163 (1982)
5. R. S. F. Chang, S. Sengupta, L. B. Shaw and N. Djeu, *SPIE Solid state lasers*, Vol. 1410, p.125 (1991)
6. R. R. Turk, "Rolling a KCl fiber: a feasibility study", *Proc. SPIE* **320**, "Advances in infrared Fibers II", 93-101 (1982).
7. B. Nayar, in Technical Digest of the Topical Meeting on integrated and Guided Wave Optics, (O.S.A. Washington D.C., 1982), paper ThA2.
8. H. E. LaBelle, *Mat. Res. Bull.* **6**, 581 (1971).
9. *J. Crystal Growth* **50**(1), (1980) is entirely devoted to shaped crystal growth, and includes a bibliography complete up to that date.
10. Y. Mimura, Y. Okamura, Y Komazawa, and C. Ota, *Japanese J. of Appl. Phys.* **19**, L269 (1980).
11. T. J. Bridges, *Optics Lett.* **5**, 85 (1980).
12. Haggerty, J. S., Final Report NASA-CR-120948 (May,1972)
13. Burris, C. A. & Stone, J., *Appl. Phys. Lett.* **26**, 318 (1975)
14. M. Fejer, J. Nightingale, G. Magel and R. L. Byer, *Rev. Sci. Instr.* **55**, 1791 (1984).
15. R. S. Feigelson, "Growth of Fiber Crystals", *Crystal Growth of Electronic Materials*, ed. by E. Kaldis, North-Holland, New York, 127-145 (1985).
16. T. Fukuda and H. Hirano, *J. Cryst. Growth* **35**, 127 (1976).
17. S. Matsumura and T. Fukuda, *J. Cryst. Growth* **34**, 350 (1976).
18. J. Stone and C. A. Burrus, *Fiber and Integrated Optics* **2**, 19 (1979).
19. U. C. Paek, *Appl. Opt.* **13**, 1383 (1974).
20. J. E. Midwinter, *Optical Fibers for Transmission*, John Wiley & Sons, New York, NY, 194 (1979).
21. W. R. Edmonds, *Appl. Opt.* **12**, 1940 (1973).
22. R. S. Feigelson, W. L. Kway and R. K. Route, *Proc. SPIE* **484**, 133 (1984)
23. J. L. Nightingale, "The Growth and Optical Applications of Single-Crystal Fibers", Ph.D. thesis, Stanford University (1985)
24. R. Mack, *Laser Focus* **23**, 122 (1987)